Neurobiology of Disease

PI4KIIIβ-Mediated Phosphoinositides Metabolism Regulates Function of the VTA Dopaminergic Neurons and Depression-Like Behavior

Yuqi Sang,[1,2,3,4*] Chenxu Niu,[1,2,3,4*] Jiaxi Xu,[1,5] Tiantian Zhu,[1,2,3,4] Shuangzhu You,[1,2,3,4] Jing Wang,[1,2,3,4] Ludi Zhang,[1,2,3,4] Xiaona Du,[1,2,3,4] and Hailin Zhang[1,2,3,4,6]

[1]Department of Pharmacology, Hebei Medical University, Shijiazhuang, Hebei 050011, China, [2]The Key Laboratory of Neural and Vascular Biology, Ministry of Education, Hebei Medical University, Shijiazhuang, Hebei 050011, China, [3]The Key Laboratory of New Drug Pharmacology and Toxicology, Hebei Medical University, Shijiazhuang, Hebei 050011, China, [4]Collaborative Innovation Center of Hebei Province for Mechanism, Diagnosis and Treatment of Neuropsychiatric Diseases, Hebei Medical University, Shijiazhuang, Hebei 050011, China, [5]Department of Physiology and Pathophysiology, Xi'an Jiaotong University Health Science Center, Xi'an, Shanxi 710061, China, and [6]Department of Psychiatry, The First Hospital of Hebei Medical University, Mental Health Institute of Hebei Medical University, Shijiazhuang, Hebei 050000, China

Phosphoinositides, including phosphatidylinositol-4,5-bisphosphate (PIP_2), play a crucial role in controlling key cellular functions such as membrane and vesicle trafficking, ion channel, and transporter activity. Phosphatidylinositol 4-kinases (PI4K) are essential enzymes in regulating the turnover of phosphoinositides. However, the functional role of PI4Ks and mediated phosphoinositide metabolism in the central nervous system has not been fully revealed. In this study, we demonstrated that PI4KIIIβ, one of the four members of PI4Ks, is an important regulator of VTA dopaminergic neuronal activity and related depression-like behavior of mice by controlling phosphoinositide turnover. Our findings provide new insights into possible mechanisms and potential drug targets for neuropsychiatric diseases, including depression. Both sexes were studied in basic behavior tests, but only male mice could be used in the social defeat depression model.

Key words: **depression; dopaminergic neurons; firing activity; phosphoinositide; PI4KIIIβ; ventral tegmental area**

Significance Statement

VTA is a brain region closely linked with mental disorders including depression. In this study, we demonstrated that PI4KIIIβ, one of the four members of PI4Ks, by controlling phosphoinositide turnover is an important regulator of the VTA DA neuronal activity and related depression-like behavior. Present results provide new angles of insights into possible mechanisms and potential drug targets for neuropsychiatric diseases including depression.

Introduction

Phosphatidylinositol 4-kinase (PI4K) is a crucial enzyme that governs the synthesis of phosphatidylinositol-4,5-bisphosphate (PIP_2; Tan and Brill, 2014; Dornan et al., 2016), a critical component of the phosphatidylinositol pathway that participates in various cellular activities such as endo- and exocytosis, cell signal transduction, cell migration, cytoskeletal protein anchoring (Yin and Janmey, 2003; Balla, 2013; Hammond and Burke, 2020), and regulation of various ion channels and transporters (Huang et al., 1998; Hilgemann et al., 2001; Runnels et al., 2002; Wu et al., 2002; Prescott and Julius, 2003; H. Zhang et al., 2003; Gamper and Shapiro, 2007; Hille et al., 2015). Anomalies in phosphoinositide metabolism and transport are implicated in the development of multiple diseases, including psychiatric and neurological disorders, T-cell deleterious, and leukemogenesis (Zhong et al., 2022).

In mammals, four subtypes of PI4K have been described, which are further categorized into type II and type III PI4K, each containing two members (PI4KIIα and PI4KIIβ, PI4KIIIα, and PI4KIIIβ; Balla, 2013). While type II PI4Ks are integrated

Received March 27, 2023; revised Dec. 18, 2023; accepted Jan. 11, 2024.

Author contributions: Y.S., C.N., J.X., T.Z., J.W., and H.Z. designed research; Y.S., C.N., J.X., T.Z., and H.Z. performed research; X.D. and H.Z. contributed unpublished reagents/analytic tools; Y.S., C.N., J.X., T.Z., S.Y., J.W., L.Z., X.D., and H.Z. analyzed data; Y.S., C.N., J.X., and H.Z. wrote the paper.

This work was supported by the National Natural Science Foundation of China (81871075, 82071533) grants to H.Z.; National Natural Science Foundation of China (U21A20359, 81870872) Grant to X.D.; Science Fund for Creative Research Groups of Natural Science Foundation of Hebei Province (H2020206474); and Basic Research Fund for Provincial Universities (JCYJ2021010).

*Y.S. and C.N. contributed equally to this work.

The authors declare no competing financial interests.

Correspondence should be addressed to Hailin Zhang at zhanghl@hebmu.edu.cn.

https://doi.org/10.1523/JNEUROSCI.0555-23.2024

membrane proteins, type III PI4Ks catalyze phosphoinositide metabolism through dynamic transit interactions with cellular membranes. Type III PI4Ks are evolutionarily and structurally related to phosphatidylinositol 3-kinase (PI3K) and can be similarly inhibited by wortmannin (Tan and Brill, 2014).

Among the PI4K isoforms, PI4KIIIβ is pivotal for PIP_2 turnover (Tabaei et al., 2016). Located in the Golgi apparatus and trans-Golgi network, PI4KIIIβ catalyzes the synthesis of phosphatidylinositol-4-phosphate (PIP; Shin and Nakayama, 2004; Balla and Balla, 2006; Tan and Brill, 2014), which is further phosphorylated into PIP_2 by phosphatidylinositol-5-phosphate. This process is essential for various cellular functions and is implicated in disease states, including virus replication and bacterial and parasite infection (Sridhar et al., 2013; Lyoo et al., 2017; Melia et al., 2017). Limited evidence has suggested the expression of PI4KIIIβ in the cerebral cortex, hippocampus, and cerebellum of rodents (Balla et al., 2000; Zólyomi et al., 2000). Mutation in the PI4KIIIβ gene is linked to SeSAME syndrome (EAST syndrome; Nadella et al., 2019), which exhibits clinical characteristics of epilepsy, ataxia, sensorineural deafness, and tubulopathy. Notably, SeSAMe is also known as a disease of channelopathy, caused by a mutation of Kir4.1 (Baba et al., 2020), a potassium channel regulated by membrane PIP_2 (Du et al., 2004).

Accumulating evidence strongly supports the involvement of dopaminergic (DA) neurons and circuits in the ventral tegmental area (VTA) in major depression (Chaudhury et al., 2013; Friedman et al., 2014; Li et al., 2017). Altered firing activity of the VTA DA neurons is directly linked to depression (Friedman et al., 2014). The underlying mechanism for these altered activities of the VTA DA neurons has been described (Friedman et al., 2014), but it is far from being fully elucidated. Considering the critical role of phosphoinositides in the modulation of ion channels (Hille et al., 2015) and the involvement of PI4KIIIβ mutation in neurological disorders identified as a channelopathy, we needed further investigation to explore the possible role of PI4KIIIβ in regulating the activity of VTA DA neurons and related behavioral functions.

Our previous studies revealed that the expression and activity of PI4KIIIβ are selectively and specifically regulated by neuronal transmitters and hormones, including norepinephrine (NE; Xu et al., 2014). This regulation possibly occurs through an enhanced interaction between PI4KIIIβ and protein kinase C (PKC; X. Zhang et al., 2010; Chen et al., 2011; Xu et al., 2014). In this study, we investigated the role of PI4KIIIβ in regulating phosphoinositide metabolism and neuronal activity in VTA DA neurons and the subsequent impact on depression-like behaviors. Our results provide evidence that PI4KIIIβ, through phosphoinositide turnover control, serves as a crucial regulator of VTA DA neuronal activity and the associated depression-like behaviors.

Methods and Materials

Animals

C57BL/6J male mice (6–10 weeks) were purchased from Vital River (Beijing, China). The mice were kept at a room temperature of 25°C and a light/dark cycle of 12 h (8:00 A.M. and 8:00 P.M.). Sufficient food and drinking water were provided. Handling of animals was in accordance with the guidelines of the Animal Care and Use Committee of Hebei Medical University and approved by the Animal Ethics Committee of Hebei Medical University. They were raised for 3 d before the experiment to adapt to the environment.

The mouse line with DA neuron-specific deletion of PI4KIIIβ ($DAT^{PI4KIIIβ-/-}$) was obtained by mating the PI4KIIIβ-loxp mice (Biocytogen) with the DA transporter (DAT)-Cre mice (Stock No. 006660, The Jackson Laboratory). The exon 4 of PI4KIIIβ (GenBank ID 656985046) was designed to be deleted under the action of a Cre enzyme. The primers for the gene typing of the $DAT^{PI4KIIIβ-/-}$ mice were as follows: Primer-F, TCTGTCCTTGCTCAGTACTTGAG, and Primer-R, CCATATCACTGAGGCCTTGAGC.

Behavior test

Mice for testing were transferred to the testing room 24 h before the test for accommodation. During the testing session, the behavior of the animals was recorded using a video tracking system and was subsequently analyzed offline. The experimenter was blinded to group identity during the experiment and quantitative analyses.

Social defeat stress. The social defeat model of depression in mice was established based on the protocols reported previously (Li et al., 2017); briefly, male C57 mice were placed in cages containing retired CD-1 mice and were attacked by the CD-1 mice for 10 min a day for 10 d. On Day 11, the sucrose preference test (SPT) was performed, and on Day 12, the social interaction test (SIT) was carried out.

The subthreshold social defeat stress. The experimental mouse was attacked by the CD1 mouse for two bouts of defeats with each bout of 2 min and interrupted by a 5 min break. The experimental mouse was then returned to its home cage and underwent a SIT the next day.

SPT. Mice were fed in a single cage and were deprived of water and food for 12 h. Each mouse was given a bottle of 0.8% sucrose solution and a bottle of purified water, which were drank freely without environmental and human interference. The consumption of sugar water and purified water in 24 h was recorded (accurately weighed), and the preference rate of sugar water in mice was calculated. Sugar water preference rate = sugar water consumption/(sugar water consumption + pure water consumption) × 100%.

SIT. The C57 mice were placed in a social cage and allowed to move freely for 2.5 min in the absence or presence of an unfamiliar caged CD1 mouse. The time the test C57 mice spent in the interaction zone was analyzed (Li et al., 2017). SIR was the social interaction time spent in the presence of CD1 mouse/in the absence of CD1 mouse. In order to enhance the stringency of our susceptibility definition, we have introduced a more stringent criterion. This revised approach necessitates not only a social interaction ratio (SIR) below 1 but also a discernible decrease in sucrose preference. To elaborate further, a reduced sucrose preference is classified as falling below the mean control (control mice) level. It is important to note that not all mice with a SIR below 1 exhibit a reduced sucrose preference. The designation of susceptibility now encompasses a combination of a SIR below 1 and a concurrent decrease in sucrose preference.

Open field test. Experiments were performed in a mouse standard open field (50 cm × 50 cm × 50 cm). During the test, the mice were placed in the center of the open field, and the free movement track of the mice in the open field and the time in the central area within 10 min were recorded.

Tail suspension test. During the test, the mouse tail was connected to the hook with medical tape, and the mice could not be stimulated in the process. Slowly hang the mice on the special hang-tail rack and start timing for 6 min. In the process, mice will show three kinds of behaviors: running state, body twisting state, and motionless state. The mice were acclimated for the first 2 min, and then the time of immobility was recorded for the next 4 min.

Elevated plus mazes. Mice were placed in the central area of the elevated plus maze (EPM) and timed for 5 min, and the time of the mice in the open arm area was recorded.

Immunofluorescence

Mice were anesthetized by pentobarbital sodium (200 mg/kg, i.p.) and perfused with 0.01 M ice-cold PBS followed by neutral 4% paraformaldehyde (PFA, Biosharp). Brains were removed and fixed in 4% PFA at 4°C

for 24 h and then dehydrated to the bottom with 30% sucrose. Embedding medium O.C.T compound (Solarbio) was used to cryoprotect the brain. Coronal frozen sections containing VTA were cut to 25 μm by a freezing microtome. In addition, 5% BSA and 0.25% triton were used for blocking and permeabilized at room temperature for 1 h. Sections were incubated with the mixture of anti-TH (1:500, mice, Merck Millipore) and anti-PI4Kb (PI4KIIIβ, 1:1,000, rabbit, Merck Millipore) antibodies at 4°C overnight, followed by the incubation with the corresponding fluorophore-conjugated secondary antibodies (Jackson ImmunoResearch Laboratories) at room temperature for 2 h in the dark. Images were acquired using a Leica TCS SP5 confocal laser microscope (Leica) or Nikon A1 (Nikon) equipped with laser lines for 405 nm, 488 nm, 561 nm, and 647 nm illumination.

Immunofluorescence analysis of PI4KIIIβ

The preparation of coronal frozen sections was as before. Sections were incubated with the mixture of anti-MAP2 (1:800, mice, Merck Millipore) and anti-PI4Kb (PI4KIIIβ, 1:1,000, rabbit, Merck Millipore) antibodies, followed by the incubation with the corresponding fluorophore-conjugated secondary antibodies (Jackson ImmunoResearch Laboratories).

To determine the relative PI4KIIIβ abundance (Table 1), the mean fluorescence intensity of PI4KIIIβ and MAP2 was measured in hemifield slices, respectively. Ratio 1 was identified as PI4KIIIβ/MAP2 in the hemisphere. Then, the average fluorescence intensity of PI4KIIIβ and MAP2 was determined in each brain region or subregion, respectively, and Ratio 2 was identified as PI4KIIIβ/MAP2 in the subregion. Calculate Ratio 2 to Ratio1, the percentage of the difference from 1 is the result. For example, when the value of Ratio 2 to Ratio 1 is 1.06, the relative abundance is 6% higher than the mean of the hemisphere.

$$\mathrm{PI4KIII\beta}(\%) = (\text{Ratio 2}/\text{Ratio 1-1}) * 100\%.$$

Western blotting

Mice were killed under anesthesia by pentobarbital sodium (100 mg/kg, i.p.), and brains were quickly removed. VTA was cut and added to RIPA lysate containing PMSF (Leagene). The tissue was homogenized and allowed to stand for 30 min and then centrifuged at 12,000 rpm for 30 min. All the above operations were carried out at 4°C. Take the supernatant and add the SDS-PAGE buffer, then maintain it at 95°C for 5 min to denature the protein. Protein samples (30 mg) were separated by 10% SDS-PAGE for 1.5 h and transferred to a polyvinylidene fluoride membrane for 2 h. The membrane was blocked by 5% skim milk powder (Sigma-Aldrich) dissolved with TBST (Biosharp) at room temperature for 2 h. Then the membrane was incubated with anti-β-actin (1:1,000, mice, Abcam) or anti-PI4Kb(PI4KIIIβ, 1:1,000, rabbit, Merck Millipore) diluted in TBST at 4°C overnight, followed incubated with corresponding secondary antibody goat anti-rabbit (1:5,000, Rockland Immunochemicals) or goat anti-mouse (1:5,000, Rockland Immunochemicals) at room temperature for 2 h in the dark. Membranes were scanned by Odyssey 9120 infrared laser imaging system (LI-COR), and the subsequent gray value density was measured and analyzed using the ImageJ software (National Institutes of Health) (Table 2).

Cannula implantation and drug delivery into VTA

Mice were anesthetized with pentobarbital sodium (50 mg/kg, i.p.) and fixed on a stereotaxic instrument. The skull was drilled, and a stainless steel sheathing cannula with a double parallel pipeline (RWD Life Science) was fixed vertically on the locator connecting rod and moved precisely to the VTA area (coordinates: anteroposterior, 3.08 mm; lateral, 0.50 mm; and dorsoventral, 4.20 mm) for implantation. Dental cement is used to secure the skull, screw, and cannula. Mice were singly housed with enough food and water to recover for 7 d. An infusion pump (RWD Life Science) was used for administration in behavior tests with a delivery rate of 100 nl/min and volume of 200 nl bilateral symmetry.

Viral injection

$DAT^{PI4KIII\beta-/-}$ mice or DAT-Cre mice were anesthetized with pentobarbital sodium (50 mg/kg, i.p) and fixed on a stereotaxic instrument (RWD Life Science). The skull was drilled, and a glass pipette was stuck into the

Table 1. Quantification of PI4KIIIβ in brain regions

Brain regions	Relative abundance of PI4KIIIβ
Telencephalon	
Olfactory system	
Main olfactory bulb	
Glomerular layer	60.30%
External plexiform layer	−12.73%
Mitral cell layer	20.17%
Internal plexiform layer	12.68%
Granule layer	15.05%
Accessory olfactory bulb	−39.05%
Anterior olfactory nucleus	−6.33%
Olfactory tubercle	−23.18%
Islands of Calleja	28.74%
Cerebral cortex	
Layer I	−42.50%
Layers II–IV	−33.21%
Layer V	−0.28%
Layer VI	−4.01%
Piriform cortex	−22.28%
Prefrontal cortex	2.17%
Hippocampal formation	
Dentate gyrus	
Granule cell layer	55.30%
Molecular layer	−7.26%
Hilus	21.20%
CA1–CA3 region	
Stratum lucidum	35.92%
Stratum radiatum	−33.53%, −24.40%
Stratum oriens	5.63%, 3.19%
Stratum pyramidale	27.79%, 73.64%
Stratum lacunosum moleculare	−27.24%
Subiculum	20.72%
Entorhinal cortex	−38.33%
Amygdala	
Central amygdaloid nucleus	15.90%
Medial amygdaloid nucleus	−46.23%
Lateral amygdaloid nucleus	−10.18%
Basolateral amygdaloid nucleus	13.36%
Basomedial amygdaloid nucleus	−25.82%
Cortical amygdaloid nuclei	−29.48%
Amygdalohippocampal area	−5.79%
Amygdalopiriform transition area	−46.96%
Nuclei of the olfactory tract	−0.85%
Substantia innominata	23.49%
Septal and basal magnocellular nuclei	
Bed nucleus stria terminalis	19.17%
Nucleus accumbens	
Core	88.90%
Shell	21.10%
Diagonal band of Broca	28.00%
Septum	
Lateral nucleus	26.19%
Medial nucleus	84.94%
Striatopallidal system	
Caudate putamen	46.10%
Globus pallidus	95.92%
Ventral pallidum	9.68%
Claustrum	−27.08%
Diencephalon	
Thalamus	
Anterior nuclei	64.42%
Lateral nuclei	85.54%
Ventral nuclei	51.02%
Mediodorsal nucleus	46.11%
Central nuclei	19.87%
Paracentral nucleus	75.81%

(*Table continues.*)

Table 1. Continued

Brain regions	Relative abundance of PI4KIIIβ
Pretectal nuclei	24.85%
Parafascicular thalamic nuclei	40.43%
Paraventricular thalamic nuclei	38.09%
Geniculate nuclei	37.09%
Reticular thalamic nucleus	26.27%
Posterior nuclear group	59.89%
Paratenial nucleus	48.98%
Rhomboid nucleus	32.39%
Ethmoid nucleus	67.25%
Reuniens	37.05%
Entopeduncular nucleus	68.6%
Subthalamic nucleus	41.53%
Zona incerta	40.89%
Habenula	
Medial	61.33%
Lateral	27.29%
Hypothalamus	
Hypothalamic areas	39.15%
Preoptic area	9.71%
Arcuate nucleus	11.40%
Supraoptic nucleus	−18.30%
Paraventricular nucleus	−9.98%
Periventricular nucleus	8.88%
Suprachiasmatic nucleus	−13.23%
Mammillary nuclei	44.35%
Brain stem	
Midbrain	
Superior colliculus	−2.93%
Inferior colliculus	20.98%
Interpeduncular nuclei	34.22%
Substantia nigra	
Pars reticulata	46.54%
Pars compacta	67.63%
Periaqueductal gray	−5.77%
Central gray	−8.18%
Raphe nuclei	
Dorsal	−3.37%
Median	33.67%
Obscurus	−29.63%
Red nucleus	53.74%
Ventral tegmental area	57.61%
Pons and medulla oblongata	
Pontine nuclei	−12.84%
Motor trigeminal nucleus	53.88%
Mesencephalic trigeminal nucleus	−17.02%
Principal sensory trigeminal nucleus	−9.01%
Spinal trigeminal nucleus	12.40%
Nucleus trapezoid body	34.69%
Locus ceruleus	−9.08%
Brachial nucleus	−15.91%
Tegmental nuclei	3.24%
Cochlear nuclei (dorsal/ventral)	−11.97%/−8.28%
Reticular nuclei	6.29%
Facial nucleus	−49.00%
Hypoglossal nucleus	15.16%
Dorsal motor nucleus of the vagus	9.00%
Ambiguus nucleus	32.86%
Cuneate nucleus	32.28%
Nucleus of the solitary tract	−8.08%
Area postrema	14.46%
Inferior olivary complex	12.22%
Lateral superior olive	6.56%
Vestibular nuclei	−21.89%
Prepositus hypoglossal nucleus	−43.56%
Cerebellum	
Molecular layer	9.29%
Purkinje cell layer	67.67%
Granule cell layer	3.12%
Deep cerebellar nuclei	3.86%

(*Table continues.*)

local VTA area (coordinates: anteroposterior, 3.08 mm; lateral, 0.50 mm; and dorsoventral, 4.20 mm) to inject 400 nl of viral AAV9-DIO-pi4kb-GFP from Vigene Biosciences (Table 2).

Sample preparation for phosphoinositide measurements using HPLC-MS
Mice were killed under anesthesia by pentobarbital sodium (100 mg/kg, i.p.), and brains were quickly removed. The VTA was cut and added to 400 µl RIPA lysate containing PMSF (Leagene) to be homogenized (60 Hz, 60 s) by a tissue grinder (Scientz). Some of the homogenates were removed for protein quantitative analysis using the method of bicinchoninic acid (BCA). The absorbance was tested at 562 nm. The protein standard (enhanced BCA protein assay kit, Beyotime) curve was established, and the protein concentration of each sample was calculated based on the standard curve. Trichloroacetic acid (TCA, 5 M) aqueous solution was added to the remaining homogenate to reach a final TCA concentration of 0.625 M. After centrifugation, the supernatant was discarded. Acidic solution for extraction of membrane phospholipid (chloroform, methanol, and 12 N hydrochloric acid = 40:80:1, v/v; 510 µl) was added to the precipitate and placed on ice for 2 h. Chloroform (170 µl) and hydrochloric acid (0.1 M, 306 µl) were added and centrifuged at low temperature (4°C, 1,500 rpm, 5 min). Take the lower organic phase into a precooled vacuum freeze dryer for 1 h. Acetonitrile–chloroform solution (1:1, v/v; 800 µl) was added to the sample, centrifuged at low temperature (4°C, 14,000 rpm, 3 min), and the supernatant 200 µl was taken for HPLC-MS measurements.

HPLC-MS conditions for measurements of phosphoinositides
Chromatographic condition:

Column: Waters XBridge C8 column (100 mm × 2.1 mm, 3.5 µm)
Guard column: sieve plate (inner diameter 2.1 mm, particle size 0.2 µm)
Column temperature: 35°C

Mobile phase:
1. Acetonitrile
2. 0.05% aqueous solution of ethylamine

Gradient elution conditions:

30% A∼80% A during 0∼3 min, A maintained at 80% during 3∼5 min, adjusted to the initial ratio after 5 min.

Flow rate: 0.4 ml/min Injection volume: 5 µl
Mass spectrum condition:

Ion source: electrospray ionization source
Detection mode: negative ion multiple reaction monitoring mode
Detected ions: m/Z: 347.9/482.5, m/Z: 347.9/283.1, m/Z = 347.9/79.0
Scan time: 100 ms
Spray voltage (IS): −4,500 V
Ion source temperature (TEM): 550°C
Atomizing gas (GS1): 55 psi
Auxiliary gas (GS2): 55 psi
Curtain air (CUR): 20 psi
Collision gas (CAD): high
Declustering voltage (DP): −35.8 V, −38.5 V, −38.6 V
Entrance voltage (EP): −10.0 V
Chamber exit voltage (CXP): −13.0 V, −5.0 V, −15.0 V

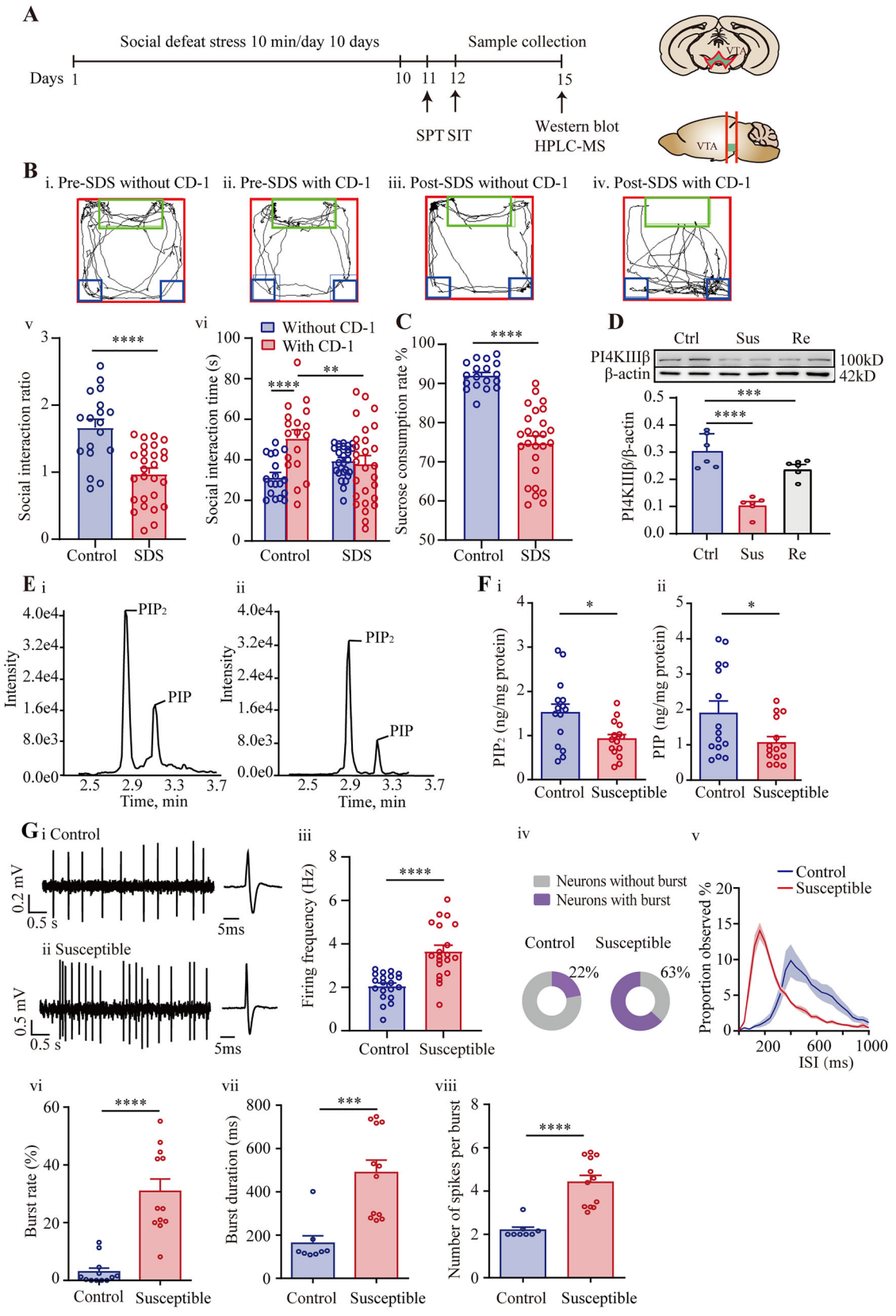

Figure 1. Continued.

Table 2. Key resources

Reagent or resource	Source	Identifier
Antibodies		
Anti-TH	Merck Millipore	AB152
Anti-PI4KIIIβ	Proteintech	13247-1-AP
Anti-MAP2	Merck Millipore	M9942
Anti-GAPDH	Abcam	AB8245
Anti-βactin	Abcam	AB8227
Bacterial and virus strains		
AAV9-DIO-pi4kb-GFP	Vigene Biosciences	N/A
Retrobeads	Lumafluor	78R170
Chemicals		
$PI(4,5)P_2$	Avanti	850165
PI(4)P	Avanti	850158
T-00127_HEV1 (T00127)	MedChemExpress	HY108313
Inositol	Merck Millipore	I5125
Cocaine hydrochloride	China National Institutes for Drug Control	N/A
Experimental models: organisms/strains		
C57BL/6J	Vital River	N/A
PI4KIIIβ-loxp	Biocytogen	LC-047
DAT-Cre	The Jackson Laboratory	006660
Software and algorithms		
GraphPad Prism 8	GraphPad Software	https://www.graphpad.com
OriginPro 9.1	OriginLab	https://www.originlab.com/
Clampfit 10.3	Molecular Devices	https://www.moleculardevices.com/

Collision energy: −10 V, −40 V, −25 V

VTA brain slice preparation

Before the experiment, the mixture of 95% O_2 and 5% CO_2 was introduced into the frozen section fluid (in mM: 220 sucrose, 2.5 KCl, 0.5 $CaCl_2$, 7 $MgCl_2$, 1.25 NaH_2PO_4, 25 $NaHCO_3$, 10 D-glucose; pH adjusted to 7.4 with HCl) to oxygen saturation, and aCSF (in mM: 124 NaCl, 3 KCl, 2 $CaCl_2$, 2 $MgCl_2$, 1.24 NaH_2PO_4, 26 $NaHCO_3$, 10 D-glucose; pH adjusted to 7.4 with HCl) was poured into the incubation tank and oxygenated to oxygen saturation at 37°C in water bath. Mice anesthetized with pentobarbital sodium (100 mg/kg, i.p.) were fixed on an anatomical plate. After the mouse heart was perfused with an oxygen-saturated frozen section solution, the brain was removed by rapid decapitation, and brain slices containing VTA with a thickness of about 200 μm were cut into slices with a vibrating microtome (VT1200S; Leica). The brain slices were placed in aCSF with continuous oxygen saturation at 37°C for 30 min, and then the incubation tank was placed at room temperature (about 25°C) for further incubation for 1 h (Li et al., 2017).

Electrophysiology and identification of DA neurons

For in vitro electrophysiological recordings, both cell-attached "loose-patch" (100–300 MΩ) and whole-cell recordings were performed to record the spontaneous firing, the membrane potential, and the whole-cell currents of DA neurons. The patch pipettes were pulled using a micropipette puller (Sutter Instrument), and the resistance was controlled to 3–5 MΩ. Electrical signals were amplified and filtered by the Axoclamp 700B preamplifier (Molecular Devices) and recorded by the Digidata 1550B AD converter (Molecular Devices). The data were analyzed by Clampfit 10.3 (Molecular Devices).

For the cell-attached "loose-patch" recordings, both the pipette and the extracellular solutions were aCSF, and the spontaneous firing of action potentials was recorded under the $I = 0$ mode. The recorded firing of action potential from the DA neuron was defined by the following characteristics: (1) a typical triphasic action potential with a negative deflection; (2) the duration of a complete action potential was >2 ms, and the width from the beginning of the firing to the minimum of hyperpolarization was >1.1 ms; (3) the firing rate was <10 Hz (Cao et al., 2010; Li et al., 2017). The presence of burst firing (as opposed to tonic firing) was identified by the following criteria: (1) the start of a burst was registered when two consecutive spikes fired within 80 ms and (2) the end of the burst was registered when the interspike interval (ISI) exceeded 160 ms (Li et al., 2017).

For the whole-cell recordings, the extracellular solution was aCSF, and the intracellular solution contained the following (in mM): 115 K-methyl sulfate, 20 KCl, 1 $MgCl_2$, and 10 HEPES (pH adjusted to 7.4 with

←

Figure 1. SDS induces depression-like behavior and downregulated expression of PI4KIIIβ and phosphoinositides in the VTA of mice. ***A***, Illustrated paradigm for SDS stimulation (left) and the location of the VTA (right). Behavior tests were performed at the time points indicated. SIT, social interaction test; SPT, sucrose preference test. Samples (the VTA) were collected at the end of the experiments. ***B***, Representative exploration traces in (i–iv). Summarized results of interaction action ratio (v), $N = 18$ and $N = 27$ for the control and SDS mice, respectively ($t_{(43)} = 4.845$, $^{****}p < 0.0001$, unpaired t test). Social interaction time (vi) for the SIT, $N = 18$ and $N = 27$ for the control and susceptible mice, respectively. Two-way (CD-1, stress) repeated measures ANOVA: CD-1, $F_{(1,43)} = 11.85$, $p = 0.0013$; stress, $F_{(1,43)} = 0.5820$, $p = 0.4497$. Bonferroni's post hoc test: significant difference between without CD-1 and with CD-1 in control mice, $^{****}p < 0.0001$, significant difference between control and SDS mice with CD-1, $^{**}p = 0.0067$). ***C***, Summarized results of sucrose consumption rate for the SPT. $N = 18$ and $N = 27$ for the control and susceptible mice, respectively ($t_{(34.24)} = 8.947$, $^{****}p < 0.0001$, Welch's t test). ***D***, Protein expression of PI4KIIIβ in the VTA measured using Western blot was quantified based on the expression level of β-actin. $N = 6$ for the control and the susceptible and the resilient mice ($F_{(2,15)} = 31.48$, $p < 0.0001$, ANOVA, Bonferroni's post hoc test: significant difference between WT and SUS mice, $^{****}p < 0.0001$). ***E***, Exemplary results of HPLC-MS measurements for PIP_2 and PIP of the control (i) and the susceptible mice (ii). ***F***, Normalized PIP_2 (i) and PIP (ii) quantity (in ng) based on the quantity of total protein level (mg) for the control and the susceptible mice. $N = 15$ for the control and the susceptible mice (i, $t_{(21.42)} = 2.687$, $^{*}p = 0.0137$, Welch's t test; ii, $t_{(20.26)} = 2.309$, $^{*}p = 0.0316$, Welch's t test). ***G***, In vivo single-unit recording of the spontaneous firing of the VTA DA neurons in control mice (i) and susceptible mice (ii), summary of firing frequency (iii), percentage of spikes in bursts during the spontaneous firing (iv), and summarized ISI of the firing spikes (v). $n = 20$, $N = 5$ for the control mice and $n = 20$, $N = 5$ for the susceptible mice ($t_{(27.92)} = 5.153$, $^{****}p < 0.0001$, Welch's t test). (vi) Burst rate ($U = 2$, $^{****}p < 0.0001$, Mann–Whitney U test), $n = 12$, $N = 5$ for the control mice and $n = 12$, $N = 5$ for the susceptible mice. (vii) Burst duration ($U = 5$, $^{***}p = 0.0003$, Mann–Whitney U test), $n = 8$, $N = 5$ for the control mice and $n = 12$, $N = 5$ for the susceptible mice. (viii) Number of spikes per burst ($U = 1$, $^{****}p < 0.0001$, Mann–Whitney U test), $n = 8$, $N = 5$ for the control mice and $n = 12$, $N = 5$ for the susceptible mice.

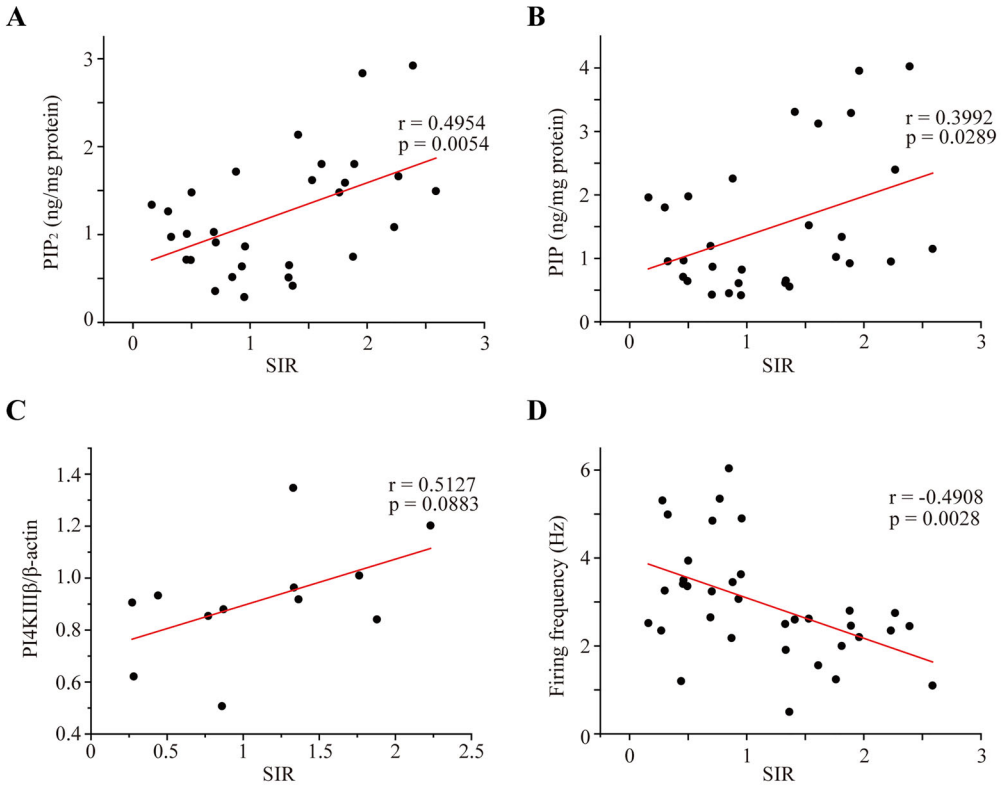

Figure 2. The correlation analysis between social interaction ratios and PI4KIIIβ levels, PIP2, PIP, and firing rate. ***A***, The correlation between SIR and PIP2. ***B***, The correlation between SIR and PI4P. ***C***, The correlation between SIR and PI4KIIIβ. ***D***, The correlation between SIR and firing frequency.

potassium hydroxide). Both spontaneous and invoked firing of action potentials (by 100 pA depolarizing currents) were recorded under current-clamp mode ($I = 0$). Inward and outward currents were also recorded using whole-cell voltage clamp mode. Currents were acquired at 10 kHz and filtered at 2.5 kHz. Series resistance (generally below 20 MΩ) was compensated by 80%. Cells were held at a holding potential of −60 mV and recorded from −120 mV to +50 mV, with a step change of 10 mV. Voltage-dependent Na^+ current was recorded using a HEKA EPC10 patch-clamp amplifier. The extracellular solution contained the following (in mM): 100 NaCl, 1.5 $MgCl_2$, 3 KCl, 2.5 $CaCl_2$, 5 HEPES, 11 D-glucose, 30 TEA-Cl, and 0.3 $CdCl_2$ (pH adjusted to 7.4 with NaOH). TEA-Cl and $CdCl_2$ were added to block both Ca^{2+} and K^+ currents. The intracellular solution contained the following (in mM): 120 CsCl, 20 TEA-Cl, 10 HEPES, and 2 $MgCl_2$ (pH adjusted to 7.4 with CsOH). Currents were acquired at 10 kHz and filtered at 2.5 kHz. Series resistance (generally below 20 MΩ) was compensated by 80%. Cells were held at a holding potential of −80 mV and recorded from −100 mV to +80 mV, with a step of 10 mV. Tetrodotoxin (TTX) 1 μM or 200 nM was added to the extracellular solution to record TTX-insensitive Na^+ current. For Kv7/M current recording, neurons were held at −25 mV, and then 1 s square pulses to −50 mV were used repeatedly with a 20 s interval. Kv7/M current was measured as the instantaneous deactivating tail current at the beginning of a voltage step to −50 mV (Koyama and Appel, 2006).

All the above cells were aspirated with the patch pipette after recording. TH and DAT were used as markers to identify DA neurons by single-cell PCR.

For in vivo electrophysiological recordings, single-unit recordings were used to record the spontaneous firing of VTA DA neurons in vivo (Mameli-Engvall et al., 2006; Li et al., 2017). Briefly, mice were intraperitoneally injected with the anesthetic pentobarbital sodium (50 mg/kg, i.p.). The recording electrodes were placed into VTA with coordinates of 2.92–3.10 mm posterior to the anterior fontanel, 0.3–0.6 mm lateral to the sagittal suture, and 4.20–5.00 mm ventral from the cortical surface. Electrical signals were amplified and filtered (10–4 KHz) by the Axoclamp 900A preamplifier and recorded by the Digidata 1440A AD converter (Molecular Devices). To observe a local effect of a drug [e.g., T00127 (10 μM)] on the spontaneous firing of VTA DA neurons, recorded in vivo using single-unit recording, we pulled a multichannel (tri-barrel) pipette on a PMP-107 multichannel micropipette puller (MicroData Instrument) and placed the pipette in the VTA with coordinates described above. Three pipette channels were used for recording firing activity and delivering the drug and the solvent control, respectively. The effect of the drug on the firing activity of the VTA DA neurons was evaluated 5 min after the drug/solvent delivery with a pressure (5–15 psi) administrator (PDES-02DX, NPI Electronic).

Single-cell PCR

PrimeScript II 1st Strand cDNA Synthesis Kit (Takara Bio) was used for reverse transcription. Briefly, 1 μl of oligo-dT (50 mM), 1 μl of deoxy-ribonucleoside triphosphate mixture (10 mM), and 2 μl of RNase-free dH_2O were added into a PCR tube. Intact cells were aspirated by the patch pipette and placed into the configured system. The system was heated to 65°C for 5 min and placed on ice to cool rapidly. Then, 2 μl of 5× PrimeScript II buffer (50 mM), 0.5 μl of RNase inhibitor (40 U/μl), 1 μl of PrimeScript II RTase (200 U/μl), and 1.5 μl of RNase-free dH_2O were added into the system. A C1000 Touch thermal cycler-CFX96 real-time PCR system was used to perform the following protocol: 50°C for 50 min and 85°C for 5 min.

Nested polymerase chain reaction was used in this case. In the first round of PCR, GoTaq Green Master Mix (Promega) and the specific "outer" primer pairs were added into the above system, and then the following protocol was performed: 95°C for 5 min, 95°C for 50 s, 58°C for 50 s, 72°C for 50 s, 30 cycles from 2 to 4, and 72°C for 10 min.

After that, the second round of PCR was carried out, and the reaction system was as follows: GoTaq Green Master Mix, the specific "inner" primer pairs, DEPC water, and 2 μl of the product of the first round of PCR (final volume, 25 μl). The protocol was 95°C for 5 min, 95°C for 50 s, 58°C or 60°C for 50 s, 72°C for 50 s, 35 cycles from 2 to 4, and 72°C for 10 min. The annealing temperature was determined by different primers.

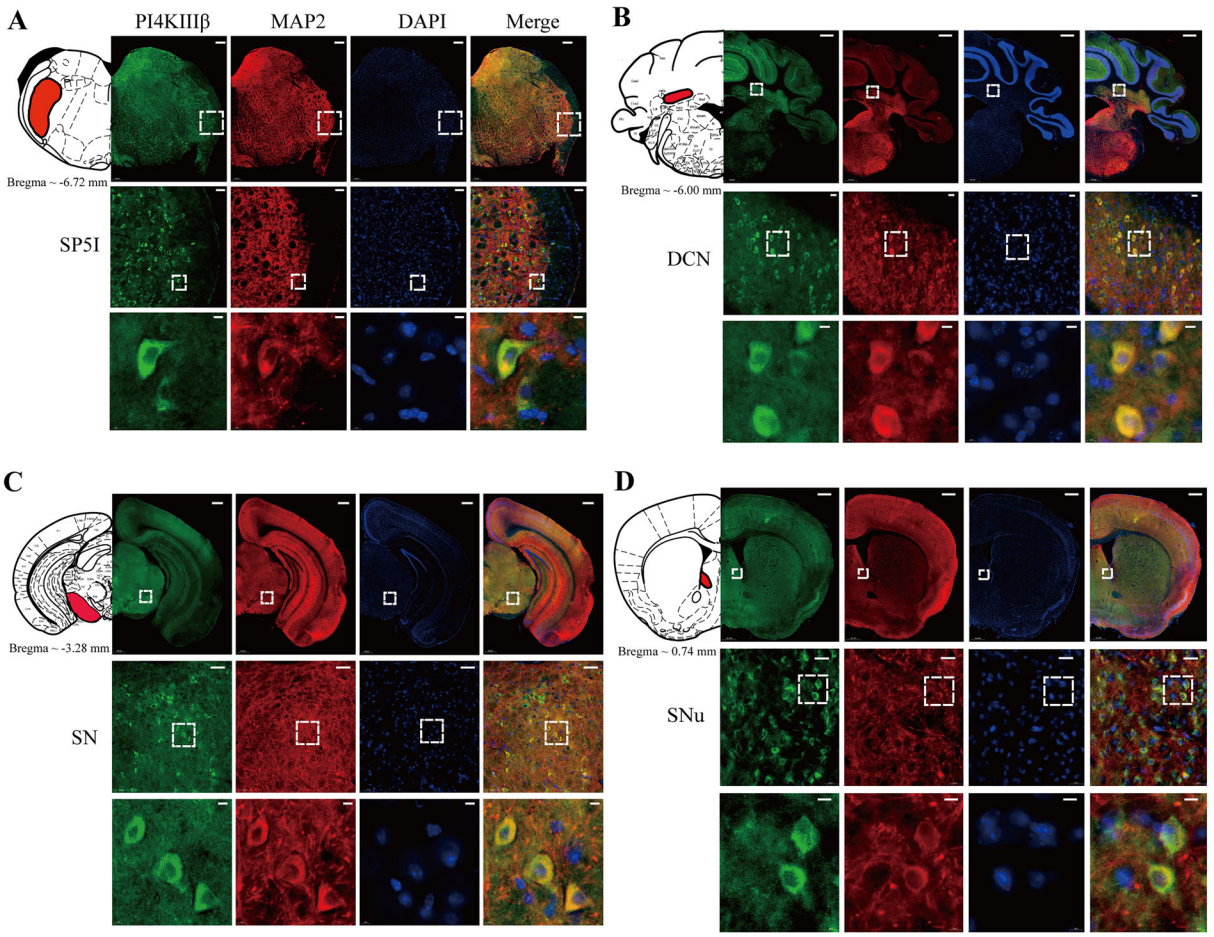

Figure 3. Representative immunofluorescence images of the whole mouse brain. ***A–D***, Representative immunofluorescence images of PI4KIIIβ, MAP2, and DAPI in SP5I, the spinal nucleus of the trigeminal; DCN, deep cerebellar nucleus; SN, substantia nigra; SNu, septal nuclei. Local magnification of the brain area is shown in the dashed box of the panoramic image, and the magnification was derived from the brain regions or nuclei shown in the red region of the brain atlas. Scale bars = 500 µm, 20 µm, and 5 µm, respectively.

Finally, the PCR reaction product was added to the prepared 2% agarose gel with ethidium bromide for electrophoresis. A gel imager was used to photograph and image.

Primers used for the nested single-cell PCR

The "outer" primers (from 5′ to 3′) are as follows:

GAPDH: Primer-F: CCAAGGTCATCCATGACAACTT
Primer-R: GAGTGGGAGTTGCTGTTGAAG
TH: Primer-F: AAGGTTCATTGGACGGCGG
Primer-R: ACATCGTCAGACACCCGAC
DAT: Primer-R: GCTCTCGGGCAGTTCAACA
Primer-R: AATGCCACGACTCTGATGGA
PI4KIIIβ: Primer-R: CTGAAGTGCACACCAACAGC
Primer-R: GGCCACCCATTACATCCACA

The "inner" primers (from 5′ to 3′) are as follows:

GAPDH: Primer-F: TGGCCTTCCGTGTTCCTAC
Primer-R: GAGTTGCTGTTGAAGTCGCA
TH: Primer-F: TCTCCTTGAGGGGTACAAAACC
Primer-R: ACCTCGAAGCGCACAAAGT
DAT: Primer-R: TACGTGGGCTTCTTCTACAATGT
Primer-R: GTTGCTGCTATGTGCATCAGA
PI4KIIIβ: Primer-R: ACAGTCACAGCTCTCCTTGC
Primer-R: TGCGTCCAGAAGGATGTTCC

Data processing and statistical analysis

SPSS 21 (IBM), GraphPad 6 (GraphPad Software), OriginPro 9.1 (OriginLab), and Illustrator (Adobe) were used for data analysis and image processing. All experimental data were expressed as mean ± SEM. Unpaired *t* test, paired *t* test, Welch's *t* test, Mann–Whitney *U* test, chi-square test, and ANOVA were used to compare the difference. For data that followed a normal distribution with homogeneous variances, unpaired *t* test and paired *t* test were applied. In cases where the data followed a normal distribution but with heterogeneous variances, Welch's *t* test was used. If the data did not conform to a normal distribution, the Mann–Whitney *U* test was chosen. Differences in proportions were compared using the chi-square test. Multiple groups were compared using one-way ANOVA. Two-way repeated measures ANOVA was used in the SIT, using genotype and stress as factors, with Bonferroni's post hoc test. Three-way repeated measures ANOVA was used in the inositol treatment test, using genotype, treatment, and time as factors, with Bonferroni's post hoc test. Significance levels were indicated as $^{*}p < 0.05$, $^{**}p < 0.01$, $^{***}p < 0.001$, and $^{****}p < 0.0001$.

Results

Social defeat stress reduces the levels of PI4KIIIβ and PIPs and increases the firing activity of the VTA DA neurons

In a preliminary study, we investigated whether PI4KIIIβ and phosphoinositides could be pharmacologically modulated by two monoamine neurotransmitters [5-hydroxytryptamine (5-HT), NE] in the VTA, a brain region closely linked to depression-like behaviors (Chaudhury et al., 2013). NE (Paladini and Williams, 2004) and 5-HT (Alex and Pehek, 2007)

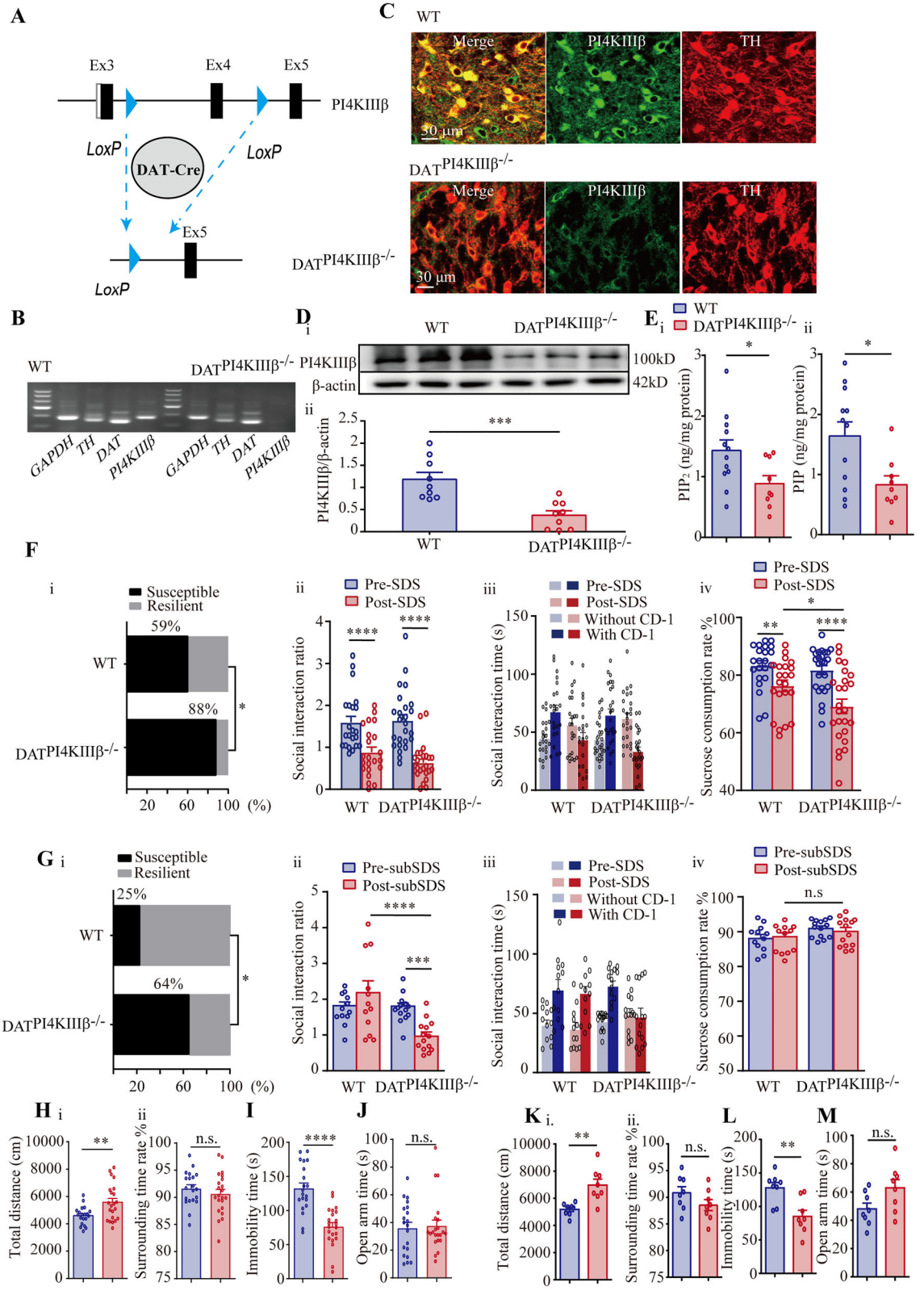

Figure 4. Continued.

have been shown to modulate the activity of midbrain DA neurons through phosphoinositides pathway-related receptors. Incubation of rat midbrain slices with NE (10 μM) or 5-HT (30 μM) for 15 min increased both total and membrane PI4KIIIβ protein levels. Accordingly, the level of PIP_2 was increased following NE and 5-HT incubations (data not presented).

Building upon our initial findings, we investigated the role of PI4KIIIβ-mediated turnover of phosphoinositides in regulating the activity of VTA DA neurons and related behaviors. To accomplish this, we established a social defeat mice model of depression following the procedure shown in Figure 1*A* (see Materials and Methods for details). We measured the SIT and SPT to assess the development of depression-like behaviors and measured levels of PI4KIIIβ protein and phosphoinositides PIP and PIP_2 from the mice VTA tissues at the end of the experiments (Fig. 1*A*). A significant reduction in the SIR (Fig. 1*Bv*) and the time spent in the interaction zone (Fig. 1*Bvi*) and in the sucrose consumption rate (Fig. 1*C*) indicated a depression-like state of the mice under continuous social defeat stress (SDS) stimulation. The mice with SIR < 1 and that exhibited a reduction in SPT were defined as susceptible (SUS) mice, whereas the mice with SIR > 1 and that did not show significant alteration in SPT were defined as resilient mice (see Materials and Methods for a detailed definition for the susceptibility).

We found that PI4KIIIβ protein from the VTA of susceptible mice was significantly reduced compared with control mice (not subjected to SDS but bred in the same environment in a time-matched manner), whereas the resilient mice did not show a significant reduction (Fig. 1*D*). Similarly, levels of PI4P and PIP_2 in the VTA, measured using HPLC-MS (Fig. 1*E*), showed a significant decrease in susceptible mice (Fig. 1*F*). Increased firing activity of VTA DA neurons is a causal factor for depression behaviors in social defeat mice (Krishnan et al., 2007). Consistent with previous findings (Li et al., 2017), both total firing frequency and burst firing activity of VTA DA neurons in susceptible mice were increased (Fig. 1*G*).

We conducted an intricate correlation analysis, delving into the interplay between PIP_2, PIP, and PI4KIIIβ levels, alongside firing frequency and interaction action ratios (Fig. 2). Our findings unveiled several significant correlations: The SIR exhibited a positive correlation with the levels of PIP_2, PIP, and PI4KIIIβ (Fig. 2*A–C*), while demonstrating a negative correlation with firing frequency (Fig. 2*D*).

Taken together, our results demonstrate that, in parallel with the development of depression-like behavior, PI4KIIIβ, PI4P, and PIP_2 in the VTA of susceptible mice were downregulated, accompanied by an increased firing activity of VTA DA neurons.

Conditional knock-out of PI4KIIIβ in DA neurons reduces the levels of PIPs and increases the susceptibility of the mice to SDS

The PI4KIIIβ protein has been shown to be expressed in the brains of mice and rats (Balla et al., 2000; Zólyomi et al., 2000), but a systematic investigation of its expression in the whole mouse brain has not yet been conducted. We used immunofluorescence staining to quantify PI4KIIIβ expression in the mouse brain, normalizing brain region-specific expression levels based on the relative fluorescence intensity of PI4KIIIβ and MAP2 (microtubule-associated protein 2, a neuron marker; Fig. 3). The results indicated that the VTA showed high levels of PI4KIIIβ expression (Table 1).

To investigate the role of PI4KIIIβ in midbrain DA neurons, we selectively deleted PI4KIIIβ in DA neurons by mating PI4KIIIβ-loxp mice with DAT-Cre mice (Fig. 4*A*). Single-cell PCR (Fig. 4*B*) and immunofluorescence staining (Fig. 4*C*) confirmed the deletion of PI4KIIIβ in DA neurons marked by DAT and TH. Western blot analysis showed a significant decrease in PI4KIIIβ protein in the VTA of the resulting mice ($DAT^{PI4KIIIβ-/-}$ mice; Fig. 4*D*), and both PIP_2 and PIP levels in the VTA were significantly reduced (Fig. 4*E*).

Behavioral tests were then conducted on the mice to assess the effects of the PI4KIIIβ deletion. Without stimulation, the SIR and sucrose preference were not significantly different between wild-type (WT) mice and $DAT^{PI4KIIIβ-/-}$ mice. However, when subjected to SDS stimulation, the $DAT^{PI4KIIIβ-/-}$ mice were more susceptible to depression-like behavior, with 88% of tested mice displaying such behavior compared with 59% of WT mice (Fig. 4*F*). In a subthreshold stress stimulation paradigm (see Materials and Methods for details), 64% of $DAT^{PI4KIIIβ-/-}$

←

Figure 4. Selective knock-out of PI4KIIIβ in the VTA DA neurons reduces phosphoinositide levels and increases the susceptibility of the mice to stress stimulation. ***A***, $PI4KIIIβ^{fl/fl}$ mice were mated with DAT-Cre mice to establish a mouse line with PI4KIIIβ being selectively deleted in the DA neurons, the $DAT^{PI4KIIIβ-/-}$ mice line. ***B***, Single-cell PCR of the VTA DA neurons in the WT and the $DAT^{PI4KIIIβ-/-}$ mice. ***C***, Immunofluorescence of the WT and the $DAT^{PI4KIIIβ-/-}$ mice, PI4KIIIβ labeling is in green, and TH labeling is in red. ***D***, Western blot results of PI4KIIIβ in the VTA. $N = 9$ for the WT and the $DAT^{PI4KIIIβ-/-}$ mice ($t_{(16)} = 4.362$, $^{***}p = 0.0005$, unpaired *t* test). ***E***, Normalized PIP_2 (i) and PIP (i) quantity (in ng) based on the quantity of total protein level (mg) for the WT and the $DAT^{PI4KIIIβ-/-}$ mice. $N = 12$ for the WT mice and $N = 9$ for the $DAT^{PI4KIIIβ-/-}$ mice (i, $t_{(19)} = 2.365$, $^{*}p = 0.0288$, unpaired *t* test; ii, $t_{(19)} = 2.689$, $^{*}p = 0.0145$, unpaired *t* test). ***F***, Proportion of susceptible or resilient mice responding to SDS stimulation (i), $N = 22$ for the WT mice and $N = 25$ for the $DAT^{PI4KIIIβ-/-}$ mice ($\chi^2 = 5.144$, $^{*}p = 0.0233$, chi-square test); SIR (ii), two-way (genotype, stress) repeated measures ANOVA: genotype, $F_{(1,45)} = 0.3607$, $p = 0.5477$; stress, $F_{(1,45)} = 286.6$, $p < 0.0001$. Bonferroni's post hoc test: significant difference between pre-SDS and post-SDS, $^{****}p < 0.0001$; social interaction time (iii); sucrose consumption rate (iv). Two-way (genotype, stress) repeated measures ANOVA: genotype, $F_{(1,45)} = 3.318$, $p = 0.0752$; stress, $F_{(1,45)} = 45.08$, $p < 0.0001$. Bonferroni's post hoc test: significant difference between pre-SDS and post-SDS, $^{**}p = 0.0037$, $^{****}p < 0.0001$; significant difference between WT and $DAT^{PI4KIIIβ-/-}$ mice, $^{*}p = 0.0259$; $N = 22$ for the WT mice and $N = 25$ for the $DAT^{PI4KIIIβ-/-}$ mice. ***G***, Proportion of susceptible or resilient mice responding to a subthreshold SDS stimulation (i), $N = 12$ for the WT mice and $N = 14$ for the $DAT^{PI4KIIIβ-/-}$ mice ($\chi^2 = 4.013$, $^{*}p = 0.0452$, chi-square test); SIR (ii). Two-way (genotype, stress) repeated measures ANOVA: genotype, $F_{(1,24)} = 7.380$, $p = 0.0120$; stress, $F_{(1,24)} = 2.780$, $p = 0.1085$. Bonferroni's post hoc test: significant difference between pre-SDS and post-SDS, $^{***}p = 0.0007$, a significant difference between WT and $DAT^{PI4KIIIβ-/-}$ mice, $^{****}p < 0.0001$; social interaction time (iii); sucrose consumption rate. Two-way (genotype, stress) repeated measures ANOVA: genotype, $F_{(1,24)} = 4.672$, $p = 0.0408$; stress, $F_{(1,24)} = 0.5928$, $p = 0.4489$. $N = 12$ for the WT mice and $N = 14$ for the $DAT^{PI4KIIIβ-/-}$ mice. ***H***, OFT of male mice. (i) The total distance traveled, $N = 20$ for the WT mice and $N = 22$ for the $DAT^{PI4KIIIβ-/-}$ mice ($t_{(31.44)} = 3.036$, $^{**}p = 0.0048$, Welch's *t* test). (ii) Percentage of time spent in the surrounding zone, $N = 20$ for the WT and $N = 22$ for the $DAT^{PI4KIIIβ-/-}$ mice ($t_{(40)} = 0.9045$, $p = 0.3711$, unpaired *t* test). ***I***, TST of male mice. Immobility time, $N = 20$ for the WT mice and $N = 22$ for the $DAT^{PI4KIIIβ-/-}$ mice ($t_{(40)} = 5.681$, $^{****}p < 0.0001$, unpaired *t* test). ***J***, Elevated plus mazes of male mice. The time spent in the open arms, $N = 20$ for the WT mice and $N = 22$ for the $DAT^{PI4KIIIβ-/-}$ mice ($U = 216.5$, $p = 0.9354$, Mann–Whitney *U* test). ***K***, OFT of female mice. (i) The total distance traveled, $N = 8$ for the WT mice and $N = 8$ for the $DAT^{PI4KIIIβ-/-}$ mice ($t_{(8.86)} = 3.83$, $^{**}p = 0.0041$, Welch's *t* test). (ii) Percentage of time spent in the surrounding zone, $N = 8$ for the WT and $N = 8$ for the $DAT^{PI4KIIIβ-/-}$ mice ($t_{(14)} = 1.521$, $p = 0.1505$, unpaired *t* test). ***L***, TST of female mice. Immobility time, $N = 8$ for the WT mice and $N = 8$ for the $DAT^{PI4KIIIβ-/-}$ mice ($t_{(14)} = 3.522$, $^{**}p = 0.0034$, unpaired *t* test). ***M***, Elevated plus mazes of female mice. The time spent in the open arms, $N = 8$ for the WT mice and $N = 8$ for the $DAT^{PI4KIIIβ-/-}$ mice ($t_{(14)} = 2.066$, $p = 0.0578$, unpaired *t* test).

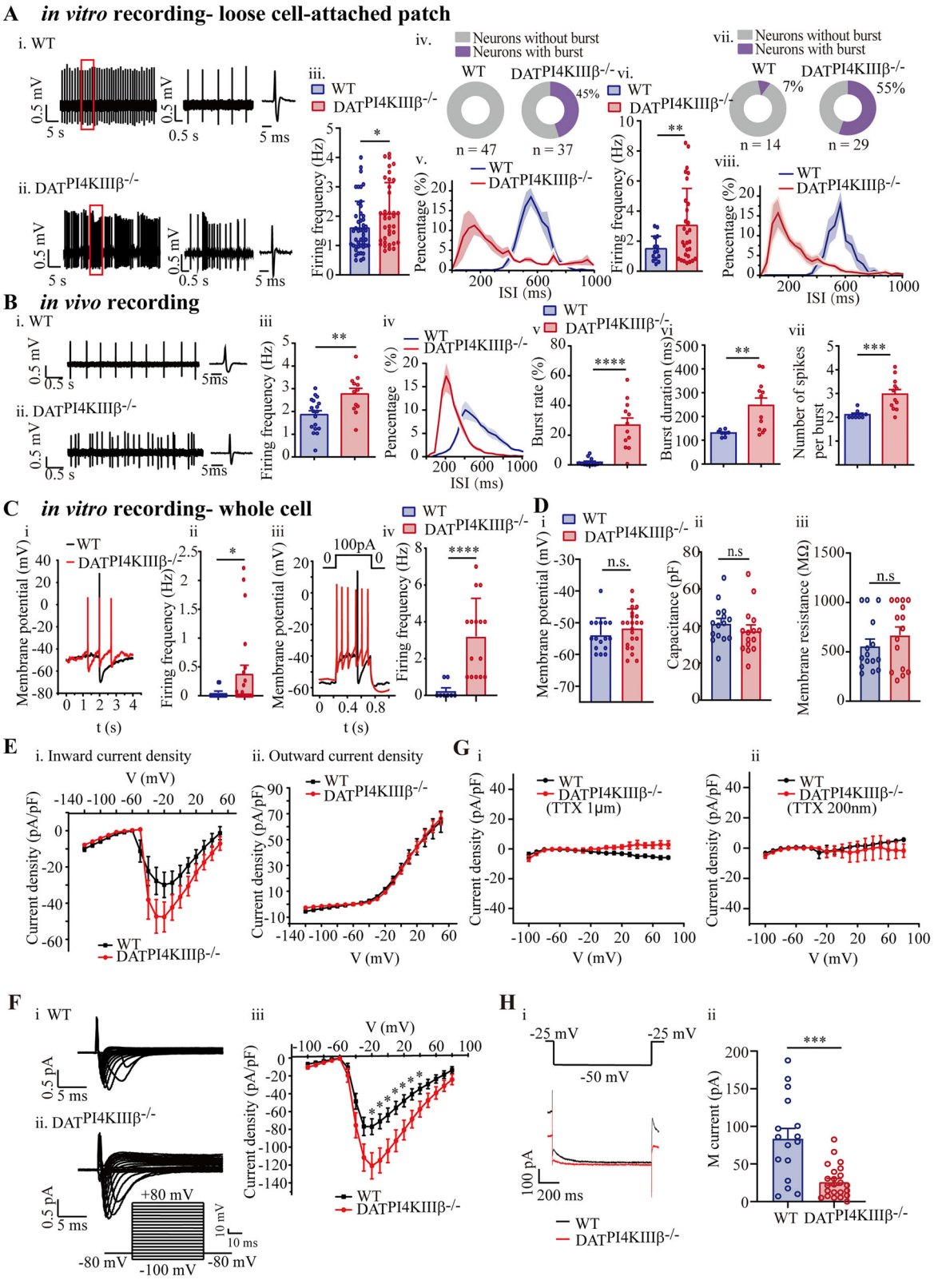

Figure 5. Continued.

mice developed depression-like behavior compared with only 25% of WT mice (Fig. 4*G*).

Additional behavioral tests were conducted on the same male and female mice, including the open field test (OFT), tested on the first day; tail suspension test (TST), tested on the second day; and EPM, tested on the third day. The $DAT^{PI4KIIIβ-/-}$ mice showed increased activity in the OFT (Fig. 4*H*) and decreased immobility time in the TST (Fig. 4*I*), indicating increased locomotor activity. No differences were observed in the EPM (Fig. 4*J*).

The experiments outlined above were exclusively conducted using male mice due to the incompatibility of defeat stimulation with female mice. Nonetheless, it is noteworthy that female $DAT^{PI4KIIIβ-/-}$ mice exhibited a parallel behavior pattern to that of their male counterparts. Specifically, these female mice displayed comparable behavioral traits, including an augmented total traveling distance in the OFT (Fig. 4*K*) and a reduction in immobility time (Fig. 4*L*). No differences were observed in the EPM (Fig. 4*M*).

These results suggest that PI4KIIIβ-mediated phosphoinositide metabolism plays a role in stress vulnerability in DA neurons. The reduction of PIP_2 and PIP levels in the VTA of $DAT^{PI4KIIIβ-/-}$ mice may contribute to their increased susceptibility to depression-like behavior under stress.

Selective deletion of PI4KIIIβ increases the firing activity of the VTA DA neurons

The firing activity and pattern of VTA DA neurons encode specific behaviors, including a depressive state (Tsai et al., 2009; Chaudhury et al., 2013). We examined the firing activity of VTA DA neurons under in vitro and in vivo conditions. Loose cell-attached patch recordings in brain slices of the VTA showed that the frequency of spontaneous firing and burst firing activity was significantly increased in $DAT^{PI4KIIIβ-/-}$ mice compared with WT mice (Fig. 5*A*); the burst firing activity, not seen in WT mice, was seen in 45% of neurons in $DAT^{PI4KIIIβ-/-}$ mice (Fig. 5*Aiv*). ISI was reduced in $DAT^{PI4KIIIβ-/-}$ mice, indicating an increase in burst activity. Particularly significant is the observation that the female $DAT^{PI4KIIIβ-/-}$ mice exhibited an elevation in the firing activity of VTA DA neurons (Fig. 5*Avi–viii*), mirroring the trends observed in male mice. In vivo single-unit recordings confirmed the increase in spontaneous firing and burst activity in VTA DA neurons of $DAT^{PI4KIIIβ-/-}$ mice (Fig. 5*B*). Whole-cell patch-clamp recordings showed increased spontaneous (Fig. 5*Ci,ii*) and induced firing activity (Fig. 5*Ciii,iv*) in $DAT^{PI4KIIIβ-/-}$ mice (Fig. 5*C*). The cell membrane potential in $DAT^{PI4KIIIβ-/-}$ mice displayed a marginal depolarization. Notably, there were no discernible differences in capacitance and membrane resistance between the WT mice and the $DAT^{PI4KIIIβ-/-}$ mice (Fig. 5*D*).

To investigate the mechanism behind the increased firing activity, we recorded whole-cell currents from VTA DA neurons. Total inward currents were increased in $DAT^{PI4KIIIβ-/-}$ mice compared with WT mice, but outward currents were not affected (Fig. 5*E*). We first focused on the inward voltage-dependent Na^+ currents since they are the major inward currents regulating VTA DA neuron excitability (Khaliq and Bean, 2010; Yang et al., 2019). The current density of inward voltage-dependent Na^+ currents was significantly increased in $DAT^{PI4KIIIβ-/-}$ mice (Fig. 5*F*), suggesting an increase in Na^+ channel conductance. TTX blocked most of the Na^+ currents, and the remaining TTX-insensitive Na^+ currents were not significantly different between $DAT^{PI4KIIIβ-/-}$ and WT mice (Fig. 5*G*), indicating that PI4KIIIβ regulates TTX-sensitive Na^+ currents, which may contribute to the increased activity of VTA DA neurons. In addition, we conducted experiments specifically targeting Kv7/M K^+ currents in both WT mice and $DAT^{PI4KIIIβ-/-}$ mice. The results have unveiled a significant reduction in Kv7/M currents in the $DAT^{PI4KIIIβ-/-}$ mice, a finding that may contribute to the heightened activity of VTA DA neurons (Fig. 5*H*).

Taken together, our results suggest that the firing activity of VTA DA neurons is regulated by PI4KIIIβ in a manner that modulates TTX-sensitive Na^+ currents and Kv7/M currents.

Pharmacologically manipulating PI4KIIIβ and phosphoinositides alters the firing activity of the VTA DA neurons and the depression-like behavior

We next aimed to investigate the effect of blockade of PI4KIIIβ activity by pharmacological means on the firing activity of the

←

Figure 5. Specific deletion of PI4KIIIβ increases spontaneous and burst firing activity of the VTA DA neurons. ***A***, In vitro cell-attached recordings of spontaneous firing of the VTA DA neurons from the WT (i) and the $DAT^{PI4KIIIβ-/-}$ mice (ii) and the summarized effects of PI4KIIIβ deletion on the firing frequency of male mice (iii), $n = 47$, $N = 10$ for the WT mice and $n = 37$, $N = 8$ for the $DAT^{PI4KIIIβ-/-}$ mice, respectively ($U = 612.5$, $^*p = 0.0201$, Mann–Whitney *U* test). (iv) Proportion of number of neurons with burst firing in the male WT mice and the $DAT^{PI4KIIIβ-/-}$ mice. (v) ISI of spontaneous firing. (vi) Summary of firing frequency of female mice, $n = 14$, $N = 4$ for the WT mice and $n = 29$, $N = 5$ for the $DAT^{PI4KIIIβ-/-}$ mice, respectively ($t_{(38.24)} = 3.044$, $^{**}p = 0.0042$, Welch's *t* test). (vii) Proportion of the number of neurons with burst firing in the female WT mice and the $DAT^{PI4KIIIβ-/-}$ mice. (viii) ISI of spontaneous firing. ***B***, In vivo single-unit recordings of spontaneously firing of the VTA DA neurons from the WT mice (i) and the $DAT^{PI4KIIIβ-/-}$ mice (ii). (iii) The summary data of firing frequency, $n = 18$, $N = 9$ for the WT mice and $n = 12$, $N = 6$ for the $DAT^{PI4KIIIβ-/-}$ mice, respectively ($t_{(28)} = 3.125$, $^{**}p = 0.0041$, unpaired *t* test). (iv) Interspike intervals of the spontaneous firing. (v) Burst rate ($U = 5$, $^{****}p < 0.0001$, Mann–Whitney *U* test), $n = 12$, $N = 5$ for the WT mice and $n = 12$, $N = 5$ for the $DAT^{PI4KIIIβ-/-}$ mice. (vi) Burst duration ($t_{(11.56)} = 3.749$, $^{**}p = 0.003$, Welch's *t* test), $n = 8$, $N = 5$ for the WT mice and $n = 12$, $N = 5$ for the $DAT^{PI4KIIIβ-/-}$ mice. (vi) Number of spikes per burst ($U = 8$, $^{***}p = 0.0009$, Mann–Whitney *U* test), $n = 8$, $N = 5$ for the WT mice and $n = 12$, $N = 5$ for the $DAT^{PI4KIIIβ-/-}$ mice. ***C***, In vitro whole-cell current-clamp recordings of spontaneous firing (i, ii) and induced firing (iii, iv) of the VTA DA neurons from brain slices of the VTA. $n = 16$, $N = 5$ for the WT mice and $n = 22$, $N = 9$, for the $DAT^{PI4KIIIβ-/-}$ mice, respectively in ii ($U = 114$, $^*p = 0.0245$, Mann–Whitney *U* test). $n = 8$, $N = 3$ for the WT mice and $n = 15$, $N = 4$ for the $DAT^{PI4KIIIβ-/-}$ mice, respectively in iv ($t_{(16.44)} = 5.261$, $^{****}p < 0.0001$, Welch's *t* test). ***D***, (i) The summary data of resting membrane potential, $n = 16$, $N = 5$ for the WT mice and $n = 22$, $N = 9$ for the $DAT^{PI4KIIIβ-/-}$ mice, respectively ($t_{(36)} = 1.131$, $p = 0.2655$, unpaired *t* test). (ii) The summary data of capacitance, $n = 15$, $N = 5$ for the WT mice and $n = 15$, $N = 5$ for the $DAT^{PI4KIIIβ-/-}$ mice, respectively ($t_{(28)} = 0.9499$, $p = 0.3503$, unpaired *t* test). (iii) The summary data of membrane resistance, $n = 15$, $N = 5$ for the WT mice and $n = 15$, $N = 5$ for the $DAT^{PI4KIIIβ-/-}$ mice, respectively ($U = 98$, $p = 0.5640$, Mann–Whitney *U* test). ***E***, Summarized inward current density (i) and outward current density (ii) of the WT (black) and the $DAT^{PI4KIIIβ-/-}$ mice (red) were shown. $n = 13$, $N = 5$ for the WT and $n = 20$, $N = 9$ for the $DAT^{PI4KIIIβ-/-}$ mice, respectively. ***F***, Voltage-dependent Na^+ current recorded in the VTA DA neurons from the brain slices of the WT mice (i) and the $DAT^{PI4KIIIβ-/-}$ mice (ii), using the protocol shown. (iii) The summary data of Na^+ current density, n = 17, N = 6 for the WT mice (black) and n = 21, N = 7 for the $DAT^{PI4KIIIβ-/-}$ mice (red), respectively (−20 mv, $t_{(31.81)} = 2.561$, $^*p = 0.0154$; −10 mv, $t_{(31.58)} = 2.702$, $^*p = 0.011$; 0 mv, $t_{(31.62)} = 2.637$, $^*p = 0.0129$; +10 mv, $t_{(31.65)} = 2.610$, $^*p = 0.0137$; +20 mv, $t_{(32.11)} = 2.556$, $^*p = 0.0155$; +30 mv, $t_{(32.68)} = 2.413$, $^*p = 0.0216$; +40 mv, $t_{(33.02)} = 2.176$, $^*p = 0.0368$, Welch's *t* test). ***G***, Na^+ currents after 1 μM (i) or 200 nM (ii) TTX, $n = 5$, $N = 2$ for the WT mice (black) and $n = 3$, $N = 2$ for the $DAT^{PI4KIIIβ-/-}$ mice (red) in i; $n = 3$, $N = 2$ for the WT mice (black) and $n = 4$, $N = 2$ for the $DAT^{PI4KIIIβ-/-}$ mice (red) in ii. ***H***, (i) Kv7/M current recorded in the VTA DA neurons from the brain slices of the WT mice and the $DAT^{PI4KIIIβ-/-}$ mice, using the protocol shown. (ii) The summary data of *M* current, $n = 16$, $N = 6$ for the WT mice and $n = 23$, $N = 7$ for the $DAT^{PI4KIIIβ-/-}$ mice, respectively ($t_{(18.18)} = 3.95$, $^{***}p = 0.0009$, Welch's *t* test).

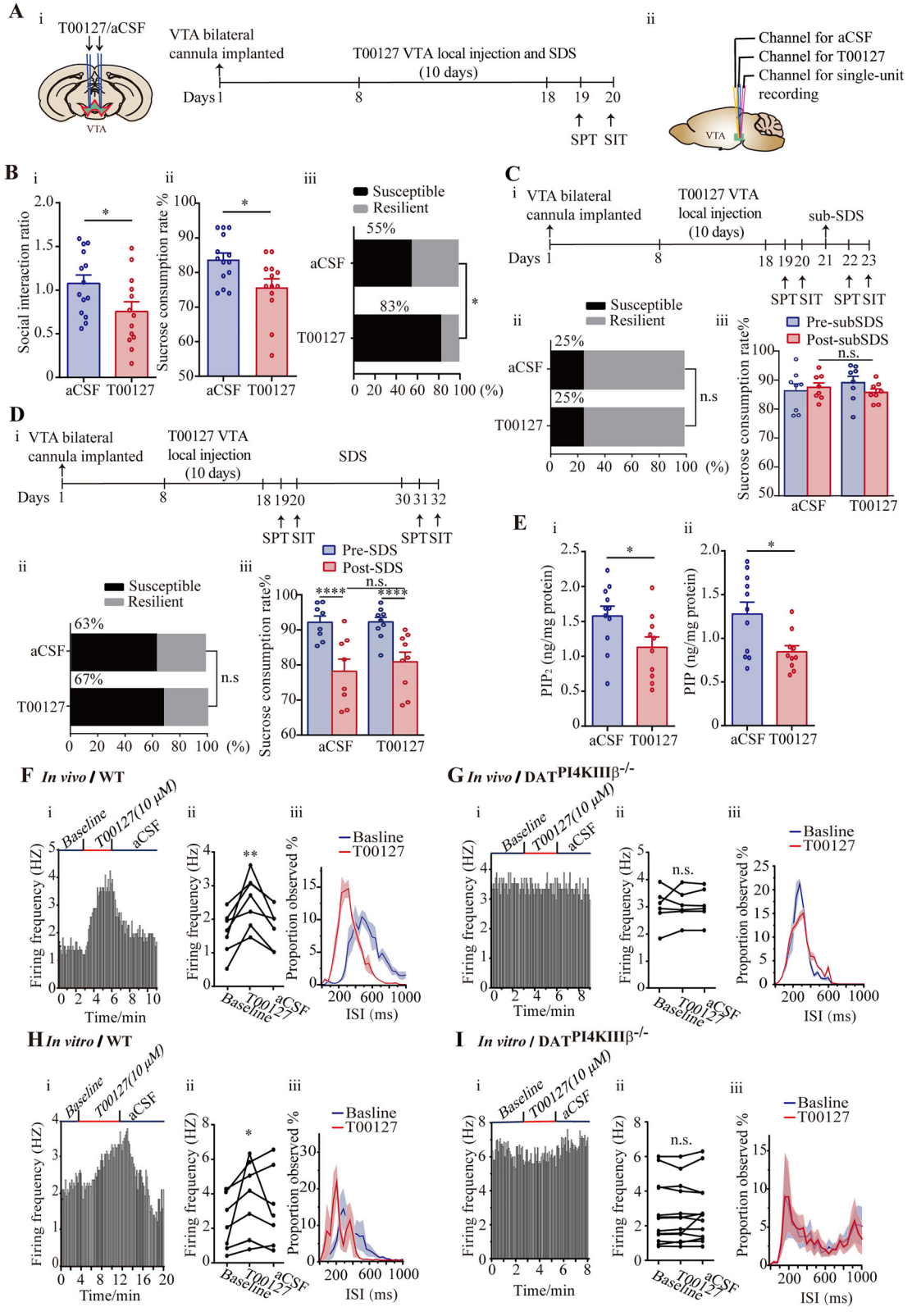

Figure 6. Continued.

VTA DA neurons and depression-like behavior. The study was conducted in three sets of experiments.

In the first set of experiments, the effects of a specific blocker of PI4KIIIβ (Arita et al., 2011; Boura and Nencka, 2015) called T00127 on depression-like behavior were tested. To accomplish this, T00127 (10 μM, 200 nl) was first applied into the VTA of mice through a cannula implanted bilaterally above the VTA, and SDS stimulation was applied to these mice after 10 min of local injection of T00127 or solvent control (artificial cerebral-spinal fluid, aCSF), for 10 d (Fig. 6*Ai*). After behavior tests of SIR and SPT, both showed declined results in the T00127-treated mice, overall demonstrating a higher susceptible rate to SDS stimulation (Fig. 6*B*).

Further experiments were conducted to investigate the influence of T00127 on the development of susceptibility in mice subjected to subthreshold stimulation. In this variation, mice received daily doses of T00127 over a span of 10 consecutive days before undergoing subthreshold stimulation (Fig. 6*Ci*). The outcomes of these experiments suggested that the continuous administration of T00127 prior to subthreshold defeat stimulation did not significantly amplify susceptibility to mild SDS (Fig. 6*Cii*). This lack of effect might be attributed to the unrestricted activity of PI4KIIIβ during exposure to subthreshold social defeat.

Additional trials explored the impact of T00127 on the susceptibility of mice when administered before full SDS stimulation. T100127 was given to mice over a span of 10 consecutive days prior to subjecting them to SDS, without continuous T00127 administration afterward (Fig. 6*Di*). The results of these experiments did not indicate any disparity in susceptibility between the control group treated with the solvent (aCSF) and the experimental group (Fig. 6*Dii*). These findings indicate that a prolonged inhibition of PI4KIIIβ using T00127 alone does not lead to an increased susceptibility in mice. However, this lack of susceptibility enhancement changes when combined with a potent SDS stimulation.

In the second set of experiments, VTA tissues were obtained from the mice 10 min after the local infusion of either T00127 or aCSF for measurements of PIP2 and PI4P levels. Both PIP_2 and PI4P levels of the VTA in the T00127-treated group were reduced (Fig. 6*E*).

In the third set of experiments, a multichannel pipette was implanted into the VTA, which was used for in vivo single-unit recording and for local T00127/aCSF delivery (Fig. 6*Aii*). Administration of T00127/aCSF significantly increased the firing frequency and the burst firing activity of the VTA DA neurons in the WT mice (Fig. 6*F,H*), which were reversed upon infusion with aCSF. Importantly, T00127 failed to affect the firing activity of the VTA DA neurons in the $DAT^{PI4KIII\beta-/-}$ mice (Fig. 6*G,I*).

In addition, inositol was tested for its effects on phosphoinositide metabolism, firing activity of the VTA DA neurons, and depression-like behaviors. Inositol was given orally in drinking water for 14 d to the mice that had been subjected to SDS simulation and had developed depression-like behaviors (Fig. 7*A*). In these SDS-susceptible mice (SUS), inositol significantly increased the levels of PI4P and PIP_2 in the VTA (Fig. 7*B*), reduced firing activity of the VTA DA neurons (Fig. 7*C*) and alleviated the depression-like behavior of WT mice but not the $DAT^{PI4KIII\beta-/-}$ mice (Fig. 7*D*). This chronic inositol treatment has no effects on locomotion or other baseline behaviors of WT mice (Fig. 7*E–G*).

Overall, the above results demonstrated that pharmacological modulation of PI4KIIIβ activity and synthesis of PIPs regulated the firing activity of the VTA DA neurons and modulated related depression-like behaviors.

Overexpression of PI4KIIIβ rescue the behavior of the $DAT^{PI4KIII\beta-/-}$ mice

Although we demonstrated above that inositol increased phosphoinositides and reduced the firing activity of VTA DA neurons, it is possible that inositol also affects depression-like behavior through targets outside of the VTA DA neurons.

To investigate the specific role of VTA DA neurons in depression-like behavior, we used AAV9-DIO-pi4kb-GFP viral particles to deliver an overexpression of PI4KIIIβ, specifically in the VTA DA neurons of mice lacking PI4KIIIβ (Fig. 8*A,B*). Western blot analysis confirmed a significant increase in PI4KIIIβ levels in the VTA of these mice (Fig. 8*C*). Phosphoinositide measurements in the affected VTA showed increased levels of PIP_2 and PIP (Fig. 8*D*). In vitro and in vivo recordings revealed that VTA DA neurons with overexpressed PI4KIIIβ fired at a lower frequency and with less bursting compared with those affected by sham viral particles (Fig. 8*E,F*).

Behavior tests were then performed on these PI4KIIIβ-overexpressed mice. No differences were observed between naive PI4KIIIβ-overexpression mice and naive sham viral particle-injected mice in their behaviors of SIR and sucrose

←

Figure 6. PI4KIIIβ blocker increases the firing activity of the VTA DA neurons and induces depression-like behavior. ***A***, (i) Schedule of the experimental procedures and schematic illustration for drug delivery. SDS stimulation and PI4KIIIβ blocker T00127 (10 μM) were applied as indicated. Behavior tests of SPT and SIT were performed at the time points indicated. (ii) A multichannel pipette was implanted into the VTA for in vivo single-unit recording and for local T00127 delivery. ***B***, The summary data for SIR (i) and sucrose consumption rate (ii), $N = 14$ for the sham group and $N = 13$ for the T00127 group (i, $t_{(25)} = 2.19$, $^*p = 0.038$, unpaired t test; ii, $t_{(25)} = 2.677$, $^*p = 0.0129$, unpaired t test). (iii) Proportion of susceptible or resilient mice responding to SDS stimulation, $N = 22$ for the sham group and $N = 23$ for the T00127 group ($\chi^2 = 4.132$, $^*p = 0.0421$, chi-square test). ***C***, (i) Schedule of the experimental procedures for the T00127 administration before subthreshold SDS stimulation. (ii) The proportion of susceptible or resilient mice responding to subthreshold SDS stimulation ($\chi^2 = 0.4103$, $p = 0.5218$, chi-square test), $N = 8$ for the aCSF group and $N = 8$ for the T00127 group. (iii) Sucrose consumption rate, two-way (blocker, stress) repeated measures ANOVA: blocker, $F_{(1,14)} = 0.0756$, $p = 0.7874$; stress, $F_{(1,14)} = 0.5094$, $p = 0.4871$. $N = 8$ for the aCSF group and $N = 8$ for the T00127 group. ***D***, (i) Schedule of the experimental procedures for the T00127 administration before SDS stimulation. (ii) The proportion of susceptible or resilient mice responding to subthreshold SDS stimulation ($\chi^2 = 0.0322$, $p = 0.8576$, chi-square test), $N = 8$ for the aCSF group and $N = 9$ for the T00127 group. (iii) Sucrose consumption rate, two-way (blocker, stress) repeated measures ANOVA: blocker, $F_{(1,15)} = 0.1505$, $p = 0.7035$; stress, $F_{(1,15)} = 127.0$, $p < 0.0001$. Bonferroni's post hoc test: significant difference between pre-SDS and post-SDS, $^{****}p < 0.0001$; $N = 8$ for the aCSF group and $N = 9$ for the T00127 group. ***E***, Normalized PIP_2 (i) and PIP (ii) quantity (in ng). $N = 11$ for aCSF and $N = 10$ for the T00127 group mice (i, $t_{(19)} = 2.2$, $^*p = 0.0404$, unpaired t test; ii, $t_{(14,82)} = 2.832$, $^*p = 0.0127$, Welch's t test). ***F***, In vivo single-unit recordings of spontaneously firing of the VTA DA neurons with local T00127 delivery by three-channel pipette in the WT mice ($n = 7$, $N = 7$). The effect of T00127 (10 μM) on the firing frequency was shown as a histogram for the time course of T00127-induced enhancement (i) and firing frequency (ii), $t_{(6)} = 3.985$, $^{**}p = 0.0072$, paired t test; effects on ISI was also shown (iii). ***G***, In vivo single-unit recording of spontaneously firing of the VTA DA neurons in the $DAT^{PI4KIII\beta-/-}$ mice ($n = 6$, $N = 6$; $t_{(5)} = 0.267$, $p = 0.8$, paired t test). ***H***, ***I***, In vitro cell-attached recordings of spontaneous firing of the VTA DA neurons from brain slice of the WT mice ($n = 7$, $N = 3$; $t_{(7)} = 2.384$, $^*p = 0.0486$, paired t test) and the $DAT^{PI4KIII\beta-/-}$ mice ($n = 13$, $N = 5$; $t_{(12)} = 0.504$, $p = 0.623$, paired t test). T00127 (10 μM) was bath applied. Effects of T00127 on ISI of spontaneous firing were also shown.

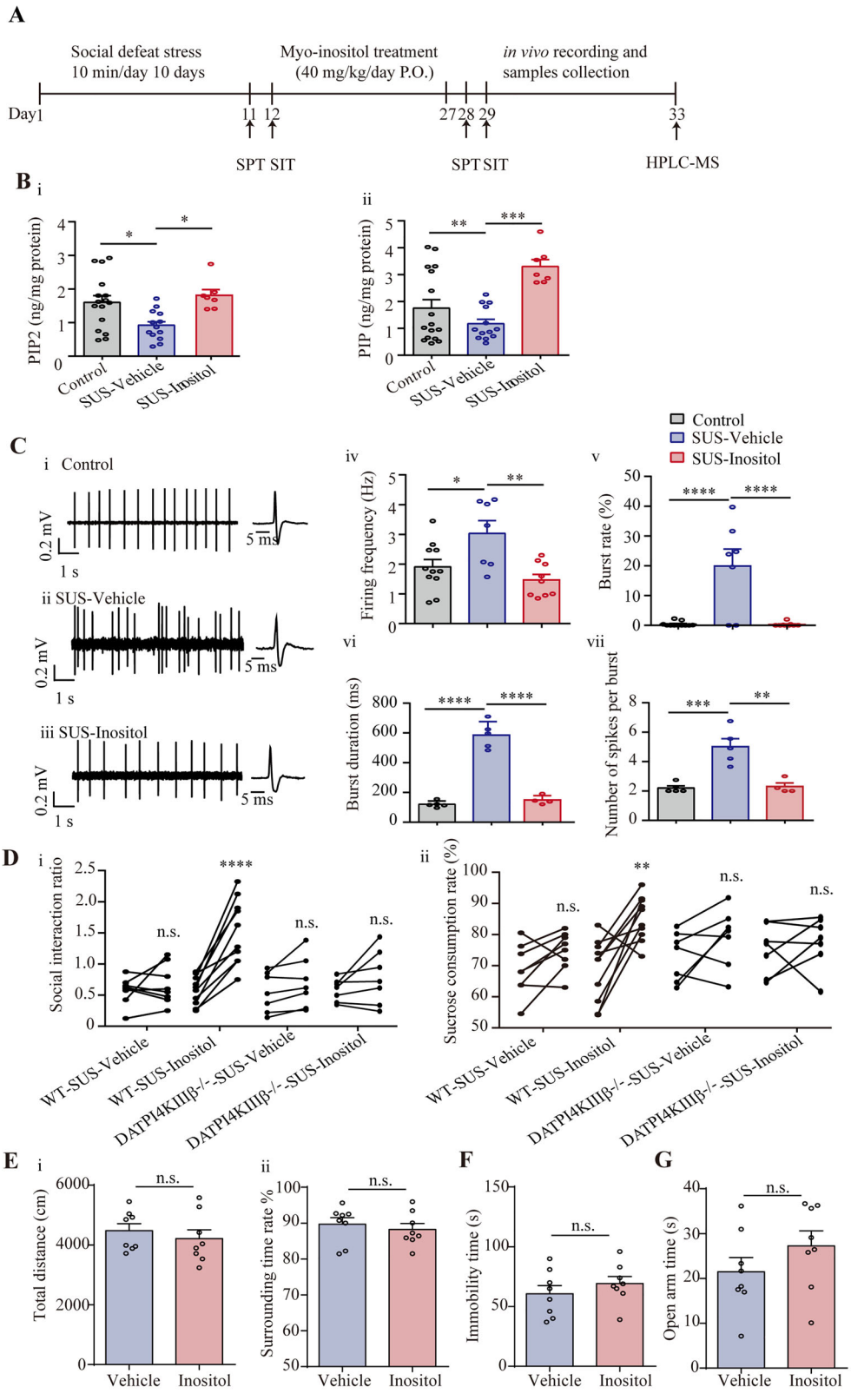

Figure 7. Continued.

consumption rate. However, after the mice were subjected to SDS, the PI4KIIIβ-overexpression mice exhibited a higher SIR and sucrose consumption rate and were more resilient to SDS (Fig. 9*A*) or subthreshold SDS (Fig. 9*B*) compared with the sham mice. The PI4KIIIβ-overexpression mice also showed reduced locomotion activity in the OFT (Fig. 9*C*) and increased immobility time in the TST (Fig. 9*D*), which reversed the increased locomotion activity and reduced TST time observed in mice lacking PI4KIIIβ (Fig. 4*H*,*I*).

However, when AAV9-DIO-pi4kb-GFP viral was injected into DAT-Cre mice, there was a minor shift toward resilience in PI4KIIIβ-overexpressing mice subjected to social defeat stimulation (from 54 to 42%), this shift does not attain statistical significance (Fig. 9*F*).

Taken together, the overexpression of PI4KIIIβ specifically in VTA DA neurons rescued altered firing activity of these neurons and the depression-like behavior and motor capability in mice lacking PI4KIIIβ.

Discussion

Our study provides compelling evidence that PI4KIIIβ-mediated phosphoinositide metabolism is a crucial regulator of midbrain VTA DA neuron activity and is implicated in DA neuron-mediated behaviors such as depression. Our findings demonstrate that PI4KIIIβ is essential for the turnover of PI4P and PIP_2 in VTA DA neurons, as selective deletion of the PI4KIIIβ gene resulted in a significant reduction of these phosphoinositides, which was reversed by reexpression of PI4KIIIβ in these neurons. Our results suggest that the VTA is among the brain regions/nuclei with a high level of PI4KIIIβ expression, consistent with its functional role as we have described.

Interestingly, although PI4KIIIβ is also expressed in other brain regions/nuclei, a PI4KIIIβ+/− mouse line with an overall deletion of PI4KIIIβ demonstrated a phenotype of increased locomotion activity in the OFT and reduced immobility time in the TST, which are behavior phenotypes similar to the $DAT^{PI4KIIIβ-/-}$ mice, suggesting a dominant functional role of PI4KIIIβ in VTA DA neurons.

Recently, a study showed that PI4KIIIα-mediated PI4P in the dendritic plasma membrane of excitatory neurons in CA1 of the hippocampus is required for neuronal activity-dependent AMPAR trafficking and long-term synaptic potentiation and memory (Guo et al., 2022). Nonetheless, we have previously demonstrated that only the activity of PI4KIIIβ in promoting the turnover of phosphoinositides was regulated by NE, a neurotransmitter and the target of antidepressants, likely through enhanced interaction between PKC and PI4KIIIβ (Chen et al., 2011; Xu et al., 2014). Therefore, PI4KIIIβ is likely the dominant isoform involved in the regulation of neuronal activity and related behaviors. Overall, PI4Ks and their mediated products of phosphoinositols should be considered important regulators of neuronal activity and related behavioral functions.

Phosphoinositides, particularly PIP_2, have been established as modulators of ion channels and transporters, which are essential elements for neuronal excitability (Prescott and Julius, 2003; Gamper and Shapiro, 2007). Therefore, the altered levels of PIP and PIP_2 observed under conditions of modulated PI4KIIIβ activity (via pharmacological or genetic means) in this study most likely contributed to the effects of PI4KIIIβ on the activity of VTA DA neurons and related behaviors. Direct evidence demonstrating the effects of phosphoinositides on neuronal excitability has been reported. For instance, altered PIP_2 dynamics and increased Kir2 currents have been shown to affect the excitability of spiny projection neurons and cause neurodevelopmental disorders (Lieberman et al., 2018). PIP_2-modulated gating of the Kv7 channel in superior cervical ganglion neurons regulates the membrane potential, neuronal excitability, and physiological functions mediated by sympathetic neurons (Kim et al., 2019).

Both intrinsic and synaptic input activities control the firing activity of VTA DA neurons (Ford, 2014; Beier et al., 2015). The present results suggest that the intrinsic ionic mechanism contributes, at least partially, to the altered activity of VTA DA neurons since in isolated in vitro brain slices of the VTA, which lack most input regulation, VTA DA neurons demonstrated similar altered firing activity as in in vivo recordings. Furthermore, the study showed that the activity of TTX-sensitive voltage-dependent Na^+ channels is enhanced in the VTA DA neurons

←

Figure 7. Inositol reduces the firing activity of VTA DA neurons and reverses the depression-like behavior. ***A***, Schedule of the experimental procedures and drug delivery. Behavior tests were performed at the time points indicated. SIT, social interaction test; SPT, sucrose preference test. The mice with both SIT and SPT showing depression-like behaviors were defined as susceptible mice (SUS) to SDS and were used for further experiments. Samples (the VTA) were collected at the end of the experiments. ***B***, Normalized PIP_2 (i) and PIP (ii) quantity (in ng). $N = 16$ for the control mice, $N = 13$ for the SUS-vehicle mice, and $N = 7$ for the SUS-inositol mice (i, $F_{(2,33)} = 6.156$, $p = 0.0053$, ANOVA, Bonferroni's post hoc test: significant difference between *control* and SUS-vehicle, $^*p = 0.0188$, significant difference between SUS-vehicle and SUS-inositol, $^*p = 0.0141$; ii, $F_{(2,33)} = 10.12$, $p = 0.0004$, ANOVA, Bonferroni's post hoc test: significant difference between *control* and SUS-vehicle, $^{**}p = 0.0067$, significant difference between SUS-vehicle and SUS-inositol, $^{***}p = 0.0003$). ***C***, In vivo single-unit recording of the spontaneous firing of the VTA DA neurons in control mice (i), SUS-vehicle mice (ii), and SUS-inositol mice (iii). (iv) Summary of firing frequency, $n = 11$, $N = 4$ for the control group; $n = 7$, $N = 4$ for the SUS-vehicle group; and $n = 9$, $N = 4$ for the SUS-inositol group ($F_{(2,24)} = 7.202$, $p = 0.0035$, ANOVA, Bonferroni's post hoc test: significant difference between *control* and SUS-vehicle, $^*p = 0.0308$, significant difference between SUS-vehicle and SUS-inositol, $^{**}p = 0.0032$). (v) Burst rate, $n = 11$, $N = 4$ for the control group; $n = 7$, $N = 4$ for the SUS-vehicle group; and $n = 9$, $N = 4$ for the SUS-inositol group ($F_{(2,24)} = 17.69$, $p < 0.0001$, ANOVA, Bonferroni's post hoc test: significant difference between *control* and SUS-vehicle, $^{****}p < 0.0001$, significant difference between SUS-vehicle and SUS-inositol, $^{****}p < 0.0001$). (vi) Burst duration, $n = 5$, $N = 4$ for the control group; $n = 5$, $N = 4$ for the SUS-vehicle group; and $n = 4$, $N = 4$ for the SUS-inositol group ($F_{(2,11)} = 98.65$, $p < 0.0001$, ANOVA, Bonferroni's post hoc test: significant difference between *control* and SUS-vehicle, $^{****}p < 0.0001$, significant difference between SUS-vehicle and SUS-inositol, $^{****}p < 0.0001$). (vii) Number of spikes per burst, $n = 5$, $N = 4$ for the control group; $n = 5$, $N = 4$ for the SUS-vehicle group; and $n = 4$, $N = 4$ for the SUS-inositol group ($F_{(2,11)} = 17.53$, $^{***}p = 0.0004$, ANOVA, Bonferroni's post hoc test: significant difference between *control* and SUS-vehicle, $^{***}p = 0.0008$, significant difference between SUS-vehicle and SUS-inositol, $^{**}p = 0.0016$). ***D***, (i) Effects of inositol on SIR, three-way (genotype, treatment, time) repeated measures ANOVA: genotype, $F_{(1,28)} = 2.691$, $p = 0.1121$; treatment, $F_{(1,28)} = 4.728$, $p = 0.0383$; time, $F_{(1,28)} = 33.75$, $p < 0.0001$. Bonferroni's post hoc test: significant difference after inositol in WT mice, $^{****}p < 0.0001$. (ii) Sucrose consumption rate, three-way (genotype, treatment, time) repeated measures ANOVA: genotype, $F_{(1,28)} = 0.8557$, $p = 0.3628$; treatment, $F_{(1,28)} = 1.552$, $p = 0.2231$; time, $F_{(1,28)} = 15.82$, $p = 0.0004$. Bonferroni's post hoc test: significant difference after inositol in WT mice, $^{**}p = 0.0014$. $N = 8$ for the WT-SUS-vehicle group, $N = 10$ for the WT-SUS-inositol group, $N = 7$ for the $DAT^{PI4KIIIβ-/-}$-SUS-vehicle group; and $N = 7$ for the $DAT^{PI4KIIIβ-/-}$-SUS-inositol group. ***E***, WT mice were treated with inositol. OFT. (i) The total distance traveled ($t_{(14)} = 0.703$, $p = 0.4936$, unpaired *t* test). (ii) Percentage of time spent in the surrounding zone ($t_{(14)} = 0.5887$, $p = 0.5654$, unpaired *t* test). $N = 8$ for the vehicle group and $N = 8$ for the inositol group. ***F***, TST. Immobility time, $N = 8$ for the vehicle group and $N = 8$ for the inositol group, respectively ($t_{(14)} = 0.9582$, $p = 0.3542$, unpaired *t* test). ***G***, Elevated plus mazes. The time spent in the open arms, $N = 8$ for the vehicle group and $N = 8$ for the inositol group, respectively ($t_{(14)} = 1.253$, $p = 0.2307$, unpaired *t* test).

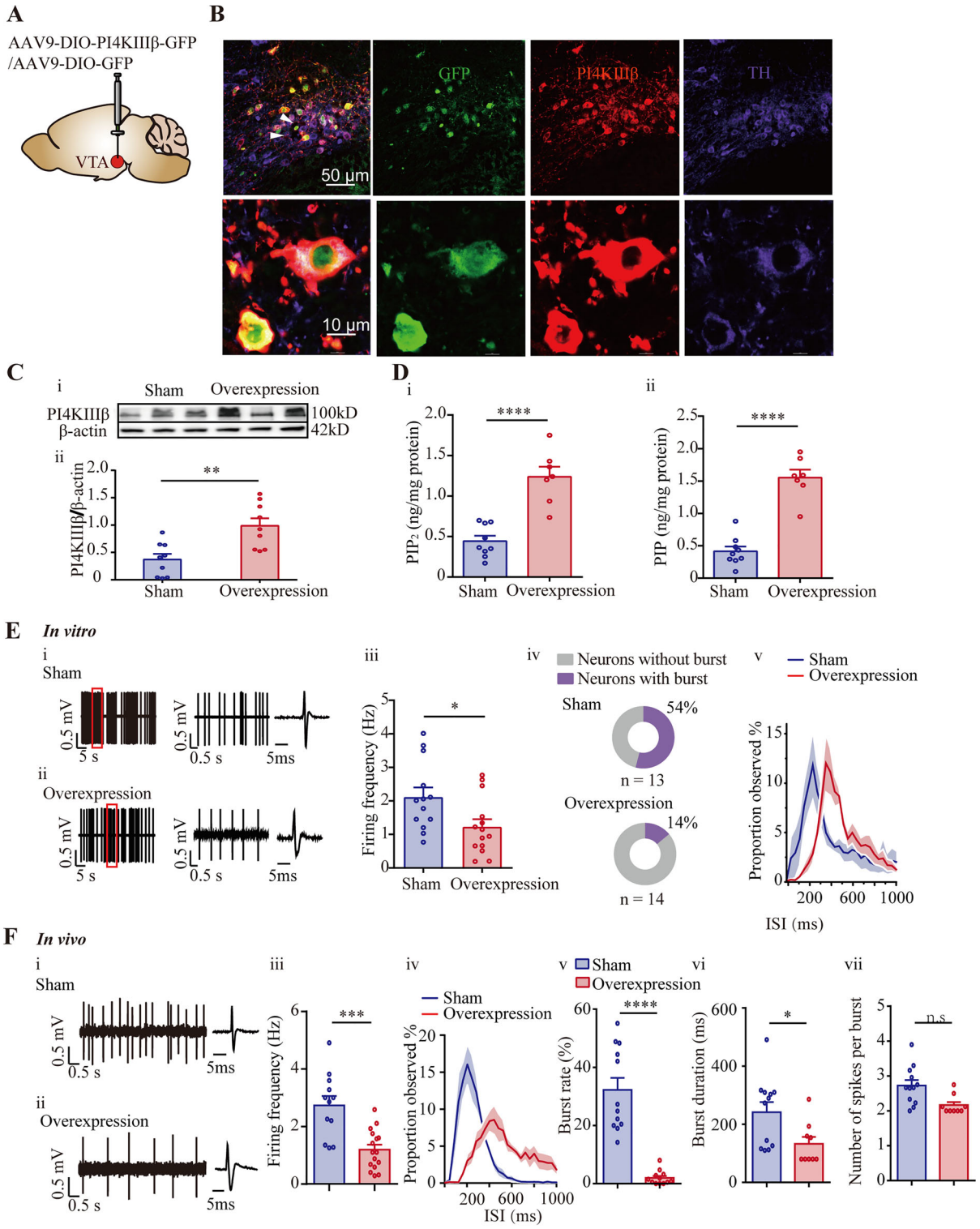

Figure 8. Overexpression of PI4KIIIβ rescues the altered PIPs and activity of the VTA DA neurons of DAT$^{PI4KIIIβ-/-}$ mice. ***A***, AAV9-DIO-PI4KIIIβ-GFP virus or sham AAV9-DIO-GFP virus was injected into the VTA of DAT$^{PI4KIIIβ-/-}$ mice. ***B***, Expression of GFP (green), PI4KIIIβ (red), and TH (purple, as a marker of DA neurons) in the VTA was visualized. ***C***, Protein expression of PI4KIIIβ in the VTA measured using Western blot was quantified based on the expression level of β-actin. $N = 9$ for the sham and the PI4KIIIβ-overexpression mice, respectively ($t_{(16)} = 3.598$, $^{**}p = 0.0024$, unpaired t test). ***D***, Normalized PIP_2 (i) and PIP (ii) quantity, $N = 9$ for the sham mice and $N = 7$ for the PI4KIIIβ-overexpression mice, respectively (i, $t_{(14)} = 5.977$, $^{****}p < 0.0001$, unpaired t test; ii, $t_{(14)} = 8.355$, $^{****}p < 0.0001$, unpaired t test). ***E***, In vitro cell-attached recordings of spontaneous firing of the VTA DA neurons. (iii) The effects of PI4KIIIβ overexpression on firing frequency, $n = 13$, $N = 5$ for the sham mice and $n = 14$, $N = 5$ for the PI4KIIIβ-overexpression mice ($t_{(25)} = 2.444$, $^{*}p = 0.0219$, unpaired t test). (iv) Proportion of the number of neurons with burst firing in the sham mice and the PI4KIIIβ-overexpression mice. (v) Internal spike intervals of the sham mice (red) and the PI4KIIIβ-overexpression mice (blue). ***F***, In vivo single-unit recordings of spontaneously firing of the VTA DA neurons, $n = 12$, $N = 5$ for the sham mice and $n = 16$, $N = 5$ for the PI4KIIIβ-overexpression mice ($t_{(26)} = 4.496$, $^{***}p = 0.0001$, unpaired t test). (iv) Internal spike intervals of the sham mice (blue) and the PI4KIIIβ-overexpression mice (red). (v) Burst rate ($U = 0$, $^{****}p < 0.0001$, Mann–Whitney U test), $n = 12$, $N = 5$ for the sham mice and $n = 12$, $N = 5$ for the overexpression mice. (vi) Burst duration ($t_{(19)} = 2.422$, $^{*}p = 0.0256$, unpaired t test), $n = 12$, $N = 5$ for the sham mice and $n = 9$, $N = 5$ for the overexpression mice. (vi) Number of spikes per burst ($U = 18$, $^{*}p = 0.079$, Mann–Whitney U test), $n = 12$, $N = 5$ for the sham mice and $n = 9$, $N = 5$ for the overexpression mice.

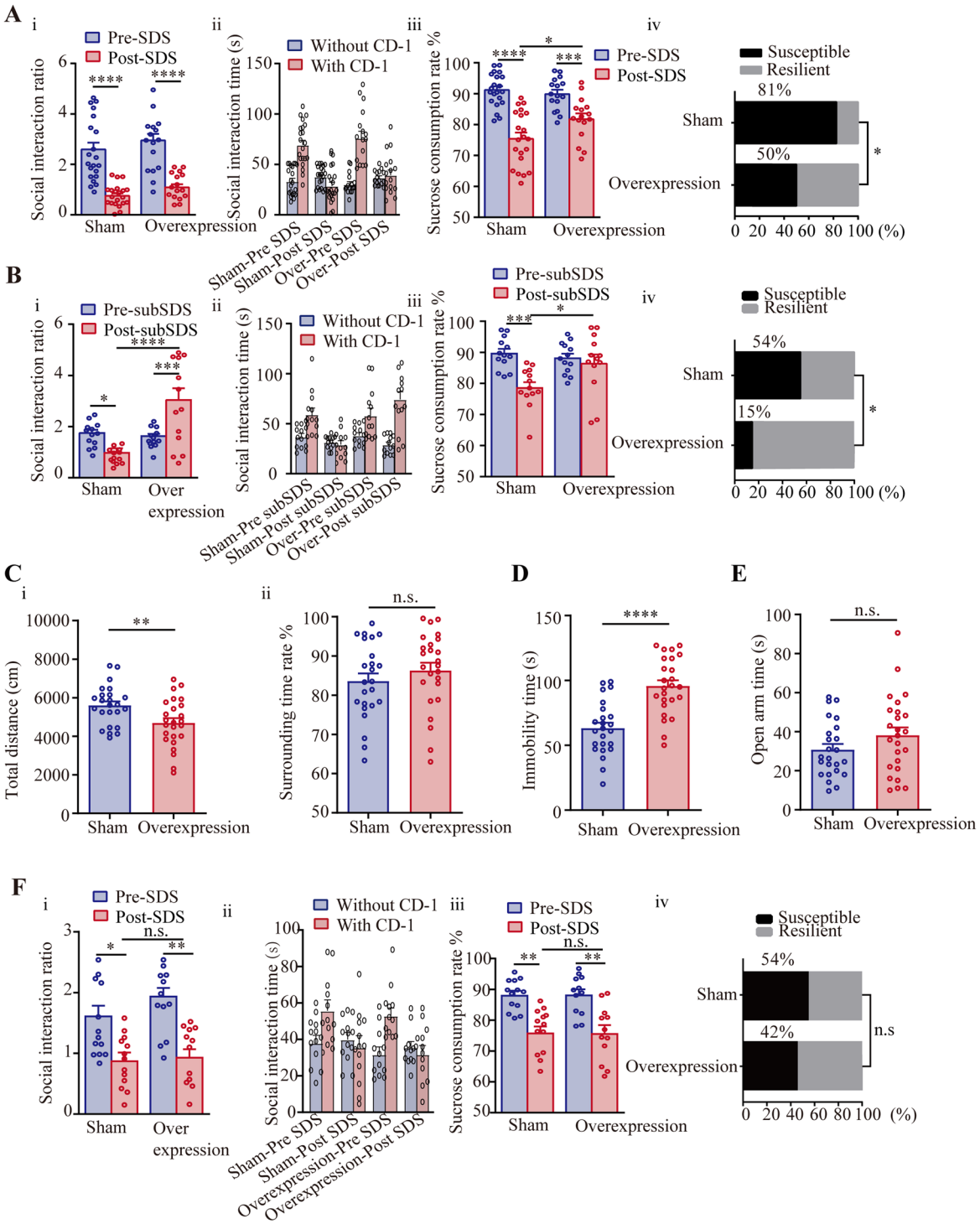

Figure 9. Continued.

of $DAT^{PI4KIII\beta-/-}$ mice, which is considered the underlying mechanism for the increased firing activity of VTA DA neurons. This is an interesting observation as PIP_2 has been shown to modulate various types of ion channels including K^+, Ca^{2+}, Cl^-, TRP channels, and ENac Na^+ channels (Hilgemann and Ball, 1996; H. Zhang et al., 1999, 2003; Ma et al., 2002; Runnels et al., 2002; Prescott and Julius, 2003; Hansen et al., 2011; Ko and Suh, 2021), but it has not been reported that voltage-dependent Na^+ channels are targets of PIP_2 (or PIP) modulation. In midbrain DA neurons, SK, Ca^{2+}, HCN (hyperpolarization-activated cyclic nucleotide-gated channel), and Kv7 channels are known to regulate excitability (Grace and Onn, 1989; Cardozo and Bean, 1995; Overton and Clark, 1997; Takada et al., 2001; Neuhoff et al., 2002), and the activity of these channels has been demonstrated to be regulated by PIP/PIP_2 (H. Zhang et al., 2003; Pian et al., 2006; M. Zhang et al., 2014; Liu et al., 2019). Our study revealed the downregulation of Kv7/M type K^+ currents in the VTA DA neurons of $DAT^{PI4KIII\beta-/-}$ mice. This decrease in K^+ channel activity, which typically serves as a regulator of neuronal activity, along with heightened depolarized inward Na^+ channel activity, likely contributes to the observed increase in firing activity of VTA DA neurons. However, further investigations are warranted to elucidate the intricate molecular mechanisms underlying the modulatory effects of PI4KIIIβ and phosphoinositols on ion channel activity expressed in VTA DA neurons.

Recent evidence has established a direct link between the firing activity of VTA DA neurons and mood behaviors, including depression and anxiety (Friedman et al., 2014; Nguyen et al., 2021; Qi et al., 2022). $DAT^{PI4KIII\beta-/-}$ mice exhibit remarkably increased firing activity in VTA DA neurons compared with WT mice, particularly increased burst firing activity, which is known to code for depression-like behaviors in the SDS model of depression (Krishnan et al., 2007; Chaudhury et al., 2013). Interestingly, $DAT^{PI4KIII\beta-/-}$ mice do not show depression-like behavior unless they are subjected to subthreshold stimulation of SDS. This result is consistent with previous reports that increased firing activity of VTA DA neurons alone is insufficient to confer depression-like behaviors in mice; only subthreshold stressful stimulation results in such behavior (Chaudhury et al., 2013). Moreover, an "antidepressant" behavior is observed in $DAT^{PI4KIII\beta-/-}$ mice in the absence of any stressful stimulation, manifested by reduced immobility time in the TST. This seemingly paradoxical result is most likely due to the increased locomotor activity of $DAT^{PI4KIII\beta-/-}$ mice, as indicated by their increased traveling distance in the OFT, which enables them to reduce immobility in the TST. This behavioral phenotype observed is similar to that induced by certain psychostimulants. For instance, cocaine, an addictive psychostimulant, is known to enhance locomotor activity in the presence of reward or during the TST, resulting in reduced immobility time (Schenk et al., 1991; Fernandez-Espejo et al., 2008). In a preliminary study, we identified a noteworthy vulnerability to cocaine in $DAT^{PI4KIII\beta-/-}$ mice. Consequently, these $DAT^{PI4KIII\beta-/-}$ mice offer a valuable resource for investigating the mechanisms underlying both physiological and pathophysiological states linked to the modulation of VTA DA neuronal excitability.

However, while we have provided compelling evidence linking the altered firing activity of VTA DA neurons to the phenotype of $DAT^{PI4KIII\beta-/-}$ mice, we must acknowledge the potential influence of PI4KIIIβ deletion on other components of the DA system that could also impact dopamine levels. Additionally, it is worth considering the potential impact of PI4KIIIβ deletion on other populations of DAT in the brain. Further investigation is necessary to comprehensively address these aspects and provide a definitive understanding of the broader effects of PI4KIIIβ deletion on the DA system.

In summary, our study reveals the role of PI4KIIIβ-mediated phosphoinositide metabolism in regulating the activity of VTA DA neurons and related depression-like behaviors. Given that phosphoinositide metabolism and pathways are modulated by several hormones and transmitters (Balla and Balla, 2006), our findings provide new insights into possible mechanisms and potential drug targets for neuropsychiatric diseases and depression.

←

Figure 9. Overexpression of PI4KIIIβ rescues the depression-like behaviors of $DAT^{PI4KIII\beta-/-}$ mice. The mice subjected to SDS stimulation. ***A***, (i) SIR, two-way (overexpression, stress) repeated measures ANOVA: overexpression, $F_{(1,35)} = 2.584$, $p = 0.1169$; stress, $F_{(1,33)} = 66.61$, $p < 0.0001$. Bonferroni's post hoc test: significant difference between pre-SDS and post-SDS, ****$p < 0.0001$. (ii) Social interaction time. (iii) Sucrose consumption rate, two-way (overexpression, stress) repeated measures ANOVA: overexpression, $F_{(1,35)} = 1.930$, $p = 0.1736$; stress, $F_{(1,35)} = 76.61$, $p < 0.0001$. Bonferroni's post hoc test: significant difference between pre-SDS and post-SDS, ****$p < 0.0001$, ***$p = 0.0007$; significant difference between sham and overexpression mice, *$p = 0.0131$. (iv) Proportion of susceptible or resilient mice responding to SDS stimulation, $N = 21$ for the sham mice and $N = 16$ for the PI4KIIIβ-overexpression mice, respectively ($\chi^2 = 3.970$, *$p = 0.0463$, chi-square test). ***B***, The mice subjected to subthreshold SDS stimulation. (i) SIR, two-way (overexpression, stress) repeated measures ANOVA: overexpression, $F_{(1,24)} = 11.26$, $p = 0.0026$; stress, $F_{(1,24)} = 1.414$, $p = 0.2460$. Bonferroni's post hoc test: significant difference between pre-subSDS and post-subSDS, *$p = 0.0212$, ***$p = 0.0003$; significant difference between sham and overexpression mice, ****$p < 0.0001$. (ii) Social interaction time. (iii) Sucrose consumption rate, two-way (overexpression, stress) repeated measures ANOVA: overexpression, $F_{(1,24)} = 2.222$, $p = 0.1490$; stress, $F_{(1,24)} = 12.05$, $p = 0.0020$. Bonferroni's post hoc test: significant difference between pre-subSDS and post-subSDS, ***$p = 0.0005$; significant difference between sham and overexpression mice, *$p = 0.0132$; (iv) proportion of susceptible or resilient mice responding to subthreshold SDS stimulation ($\chi^2 = 4.248$, *$p = 0.0393$, chi-square test). $N = 13$ for the sham mice and $N = 13$ for the PI4KIIIβ-overexpression mice. ***C***, OFT. (i) The total distance traveled ($t_{(47)} = 2.739$, **$p = 0.0087$, unpaired t test). (ii) Percentage of time spent in the surrounding zone ($t_{(47)} = 0.9793$, $p = 0.3324$, unpaired t test). $N = 24$ for the sham mice and $N = 25$ for the overexpression mice. ***D***, TST. Immobility time ($t_{(47)} = 5.32$, ****$p < 0.0001$, unpaired t test). $N = 24$ for the sham mice and $N = 25$ for the overexpression mice. ***E***, Elevated plus mazes. The time spent in the open arms ($t_{(47)} = 1.481$, $p = 0.1452$, unpaired t test). $N = 24$ for the sham mice and $N = 25$ for the overexpression mice. ***F***, AAV9-DIO-PI4KIIIβ-GFP virus or sham AAV9-DIO-GFP virus was injected into the VTA of DAT-Cre mice and subjected to SDS stimulation. (i) SIR, two-way (overexpression, stress) repeated measures ANOVA: overexpression, $F_{(1,23)} = 4.941$, $p = 0.0363$; stress, $F_{(1,23)} = 17.57$, $p = 0.0003$. Bonferroni's post hoc test: significant difference between pre-SDS and post-SDS, *$p = 0.0377$, **$p = 0.0051$. (ii) Social interaction time. (iii) Sucrose consumption rate, two-way (overexpression, stress) repeated measures ANOVA: overexpression, $F_{(1,23)} = 0.0570$, $p = 0.8134$; stress, $F_{(1,23)} = 32.24$, $p < 0.0001$. Bonferroni's *post hoc* test: significant difference between pre-SDS and post-SDS, **$p = 0.0011$, **$p = 0.0010$; (iv) proportion of susceptible or resilient mice responding to SDS stimulation ($\chi^2 = 0.3708$, $p = 0.5425$, chi-square test). $N = 13$ for the sham mice and $N = 12$ for the PI4KIIIβ-overexpression mice.

References

Alex KD, Pehek EA (2007) Pharmacologic mechanisms of serotonergic regulation of dopamine neurotransmission. Pharmacol Ther 113:296–320.

Arita M, Kojima H, Nagano T, Okabe T, Wakita T, Shimizu H (2011) Phosphatidylinositol 4-kinase III beta is a target of enviroxime-like compounds for antipoliovirus activity. J Virol 85:2364–2372.

Baba T, Alvarez-Prats A, Kim YJ, Abebe D, Wilson S, Aldworth Z, Stopfer MA, Heuser J, Balla T (2020) Myelination of peripheral nerves is controlled by PI4KB through regulation of Schwann cell Golgi function. Proc Natl Acad Sci U S A 117:28102–28113.

Balla T (2013) Phosphoinositides: tiny lipids with giant impact on cell regulation. Physiol Rev 93:1019–1137.

Balla A, Balla T (2006) Phosphatidylinositol 4-kinases: old enzymes with emerging functions. Trends Cell Biol 16:351–361.

Balla A, Vereb G, Gülkan H, Gehrmann T, Gergely P, Heilmeyer LM Jr, Antal M (2000) Immunohistochemical localisation of two phosphatidylinositol 4-kinase isoforms, PI4K230 and PI4K92, in the central nervous system of rats. Exp Brain Res 134:88–279.

Beier KT, Steinberg EE, DeLoach KE, Xie S, Miyamichi K, Schwarz L, Gao XJ, Kremer EJ, Malenka RC, Luo L (2015) Circuit architecture of VTA dopamine neurons revealed by systematic input-output mapping. Cell 162: 622–634.

Boura E, Nencka R (2015) Phosphatidylinositol 4-kinases: function, structure, and inhibition. Exp Cell Res 337:136–145.

Cao JL, Covington HE 3rd, Friedman AK, Wilkinson MB, Walsh JJ, Cooper DC, Nestler EJ, Han MH (2010) Mesolimbic dopamine neurons in the brain reward circuit mediate susceptibility to social defeat and antidepressant action. J Neurosci 30:16453–16458.

Cardozo DL, Bean BP (1995) Voltage-dependent calcium channels in rat midbrain dopamine neurons: modulation by dopamine and GABAB receptors. J Neurophysio 74:1137–1148.

Chaudhury D, et al. (2013) Rapid regulation of depression-related behaviours by control of midbrain dopamine neurons. Nature 493:532–536.

Chen X, Zhang X, Jia C, Xu J, Gao H, Zhang G, Du X, Zhang H (2011) Membrane depolarization increases membrane PtdIns(4,5)P2 levels through mechanisms involving PKC βII and PI4 kinase. J Biol Chem 286:39760–39767.

Dornan GL, McPhail JA, Burke JE (2016) Type III phosphatidylinositol 4 kinases: structure, function, regulation, signalling and involvement in disease. Biochem Soc Trans 44:260–266.

Du X, Zhang H, Lopes C, Mirshahi T, Rohacs T, Logothetis DE (2004) Characteristic interactions with phosphatidylinositol 4,5-bisphosphate determine regulation of kir channels by diverse modulators. J Biol Chem 279:37271–37281.

Fernandez-Espejo E, Ramiro-Fuentes S, Portavella M, Moreno-Paublete R (2008) Role for D-serine within the ventral tegmental area in the development of cocaine's sensitization. Neuropsychopharmacology 33: 995–1003.

Ford CP (2014) The role of D2-autoreceptors in regulating dopamine neuron activity and transmission. Neuroscience 282:13–22.

Friedman AK, et al. (2014) Enhancing depression mechanisms in midbrain dopamine neurons achieves homeostatic resilience. Science 344:313–319.

Gamper N, Shapiro MS (2007) Regulation of ion transport proteins by membrane phosphoinositides. Nat Rev Neurosci 8:921–934.

Grace AA, Onn SP (1989) Morphology and electrophysiological properties of immunocytochemically identified rat dopamine neurons recorded in vitro. J Neurosci 9:3463–3481.

Guo Z, et al. (2022) Activity-dependent PI4P synthesis by PI4KIIIα regulates long-term synaptic potentiation. Cell Rep 38:110452.

Hammond G, Burke JE (2020) Novel roles of phosphoinositides in signaling, lipid transport, and disease. Curr Opin Cell Biol 63:57–67.

Hansen SB, Tao X, MacKinnon R (2011) Structural basis of PIP2 activation of the classical inward rectifier K+ channel Kir2.2. Nature 477:495–498.

Hilgemann DW, Ball R (1996) Regulation of cardiac Na+, Ca2+ exchange and KATP potassium channels by PIP2. Science 273:956–959.

Hilgemann DW, Feng S, Nasuhoglu C (2001) The complex and intriguing lives of PIP2 with ion channels and transporters. Sci STKE 2001:re19.

Hille B, Dickson EJ, Kruse M, Vivas O, Suh BC (2015) Phosphoinositides regulate ion channels. Biochim Biophys Acta 1851:844–856.

Huang CL, Feng S, Hilgemann DW (1998) Direct activation of inward rectifier potassium channels by PIP2 and its stabilization by Gβγ. Nature 391: 803–806.

Khaliq ZM, Bean BP (2010) Pacemaking in dopaminergic ventral tegmental area neurons: depolarizing drive from background and voltage-dependent sodium conductances. J Neurosci 30:7401–7413.

Kim KW, Kim K, Lee H, Suh BC (2019) Ethanol elevates excitability of superior cervical ganglion neurons by inhibiting Kv7 channels in a cell type-specific and PI(4,5)P(2)-dependent manner. Int J Mol Sci 20:4419.

Ko W, Suh BC (2021) Differential regulation of Ca(2+)-activated Cl(-) channel TMEM16A splice variants by membrane PI(4,5)P(2). Int J Mol Sci 22: 4088.

Koyama S, Appel SB (2006) Characterization of M-current in ventral tegmental area dopamine neurons. J Neurophysiol 96:535–543.

Krishnan V, et al. (2007) Molecular adaptations underlying susceptibility and resistance to social defeat in brain reward regions. Cell 131:391–404.

Li L, et al. (2017) Selective targeting of M-type potassium K(v) 7.4 channels demonstrates their key role in the regulation of dopaminergic neuronal excitability and depression-like behaviour. Br J Pharmacol 174:4277–4294.

Lieberman OJ, McGuirt AF, Mosharov EV, Pigulevskiy I, Hobson BD, Choi S, Frier MD, Santini E, Borgkvist A, Sulzer D (2018) Dopamine triggers the maturation of striatal spiny projection neuron excitability during a critical period. Neuron 99:540–554.e4.

Liu Y, Iwano T, Ma F, Wang P, Wang Y, Zheng M, Liu G, Ono K (2019) Short- and long-term roles of phosphatidylinositol 4,5-bisphosphate PIP(2) on Cav3.1- and Cav3.2-T-type calcium channel current. Pathophysiology 26:31–38.

Lyoo H, Dorobantu CM, van der Schaar HM, van Kuppeveld F (2017) Modulation of proteolytic polyprotein processing by coxsackievirus mutants resistant to inhibitors targeting phosphatidylinositol-4-kinase IIIβ or o xysterol binding protein. Antiviral Res 147:86–90.

Ma HP, Saxena S, Warnock DG (2002) Anionic phospholipids regulate native and expressed epithelial sodium channel (ENaC). J Biol Chem 277:7641–7644.

Mameli-Engvall M, Evrard A, Pons S, Maskos U, Svensson TH, Changeux JP, Faure P (2006) Hierarchical control of dopamine neuron-firing patterns by nicotinic receptors. Neuron 50:911–921.

Melia CE, et al. (2017) Escaping host factor PI4KB inhibition: enterovirus genomic RNA replication in the absence of replication organelles. Cell Rep 21:587–599.

Nadella RK, et al. (2019) Identification and functional characterization of two novel mutations in KCNJ10 and PI4KB in SeSAME syndrome without electrolyte imbalance. Hum Genomics 13:53.

Neuhoff H, Neu A, Liss B, Roeper J (2002) I(h) channels contribute to the different functional properties of identified dopaminergic subpopulations in the midbrain. J Neurosci 22:1290–1302.

Nguyen C, et al. (2021) Nicotine inhibits the VTA-to-amygdala dopamine pathway to promote anxiety. Neuron 109:2604–2615.e9.

Overton PG, Clark D (1997) Burst firing in midbrain dopaminergic neurons. Brain Res Brain Res Rev 25:312–334.

Paladini CA, Williams JT (2004) Noradrenergic inhibition of midbrain dopamine neurons. J Neurosci 24:4568–4575.

Pian P, Bucchi A, Robinson RB, Siegelbaum SA (2006) Regulation of gating and rundown of HCN hyperpolarization-activated channels by exogenous and endogenous PIP2. J Gen Physiol 128:593–604.

Prescott ED, Julius D (2003) A modular PIP2 binding site as a determinant of capsaicin receptor sensitivity. Science 300:1284–1288.

Qi G, et al. (2022) NAc-VTA circuit underlies emotional stress-induced anxiety-like behavior in the three-chamber vicarious social defeat stress mouse model. Nat Commun 13:577.

Runnels LW, Yue L, Clapham DE (2002) The TRPM7 channel is inactivated by PIP(2) hydrolysis. Nat Cell Biol 4:329–336.

Schenk S, Snow S, Horger BA (1991) Pre-exposure to amphetamine but not nicotine sensitizes rats to the motor activating effect of cocaine. Psychopharmacology 103:62–66.

Shin HW, Nakayama K (2004) Dual control of membrane targeting by PtdIns(4)P and ARF. Trends Biochem Sci 29:513–515.

Sridhar S, Patel B, Aphkhazava D, Macian F, Santambrogio L, Shields D, Cuervo AM (2013) The lipid kinase PI4KIIIβ preserves lysosomal identity. EMBO J 32:324–339.

Tabaei SR, Guo F, Rutaganira FU, Vafaei S, Choong I, Shokat KM, Glenn JS, Cho NJ (2016) Multistep compositional remodeling of supported lipid membranes by interfacially active phosphatidylinositol kinases. Anal Chem 88:5042–5045.

Takada M, Kang Y, Imanishi M (2001) Immunohistochemical localization of voltage-gated calcium channels in substantia nigra dopamine neurons. Eur J Neurosci 13:757–762.

Tan J, Brill JA (2014) Cinderella story: PI4P goes from precursor to key signaling molecule. Crit Rev Biochem Mol Biol 49:33–58.

Tsai HC, Zhang F, Adamantidis A, Stuber GD, Bonci A, de Lecea L, Deisseroth K (2009) Phasic firing in dopaminergic neurons is sufficient for behavioral conditioning. Science 324:1080–1084.

Wu L, Bauer CS, Zhen XG, Xie C, Yang J (2002) Dual regulation of voltage-gated calcium channels by PtdIns(4,5)P2. Nature 419:947–952.

Xu JX, Si M, Zhang HR, Chen XJ, Zhang XD, Wang C, Du XN, Zhang HL (2014) Phosphoinositide kinases play key roles in norepinephrine- and angiotensin II-induced increase in phosphatidylinositol 4,5-bisphosphate and modulation of cardiac function. J Biol Chem 289:6941–6948.

Yang J, Xiao Y, Li L, He Q, Li M, Shu Y (2019) Biophysical properties of somatic and axonal voltage-gated sodium channels in midbrain dopaminergic neurons. Front Cell Neurosci 13:317.

Yin HL, Janmey PA (2003) Phosphoinositide regulation of the actin cytoskeleton. Annu Rev Physiol 65:761–789.

Zhang X, Chen X, Jia C, Geng X, Du X, Zhang H (2010) Depolarization increases phosphatidylinositol (PI) 4,5-bisphosphate level and KCNQ currents through PI 4-kinase mechanisms. J Biol Chem 285: 9402–9409.

Zhang H, Craciun LC, Mirshahi T, Rohács T, Lopes CM, Jin T, Logothetis DE (2003) PIP(2) activates KCNQ channels, and its hydrolysis underlies receptor-mediated inhibition of M currents. Neuron 37:963–975.

Zhang H, He C, Yan X, Mirshahi T, Logothetis DE (1999) Activation of inwardly rectifying K+ channels by distinct PtdIns(4,5)P2 interactions. Nat Cell Biol 1:183–188.

Zhang M, Meng XY, Cui M, Pascal JM, Logothetis DE, Zhang JF (2014) Selective phosphorylation modulates the PIP2 sensitivity of the CaM-SK channel complex. Nat Chem Biol 10:753–759.

Zhong W, et al. (2022) An acquired phosphatidylinositol 4-phosphate transport initiates T-cell deterioration and leukemogenesis. Nat Commun 13: 4390.

Zólyomi A, Zhao X, Downing GJ, Balla T (2000) Localization of two distinct type III phosphatidylinositol 4-kinase enzyme mRNAs in the rat. Am J Physiol Cell Physiol 278:C914–C920.